Article

Neuron

Time Cells in the Hippocampus Are Neither Dependent on Medial Entorhinal Cortex Inputs nor Necessary for Spatial Working Memory

Graphical Abstract

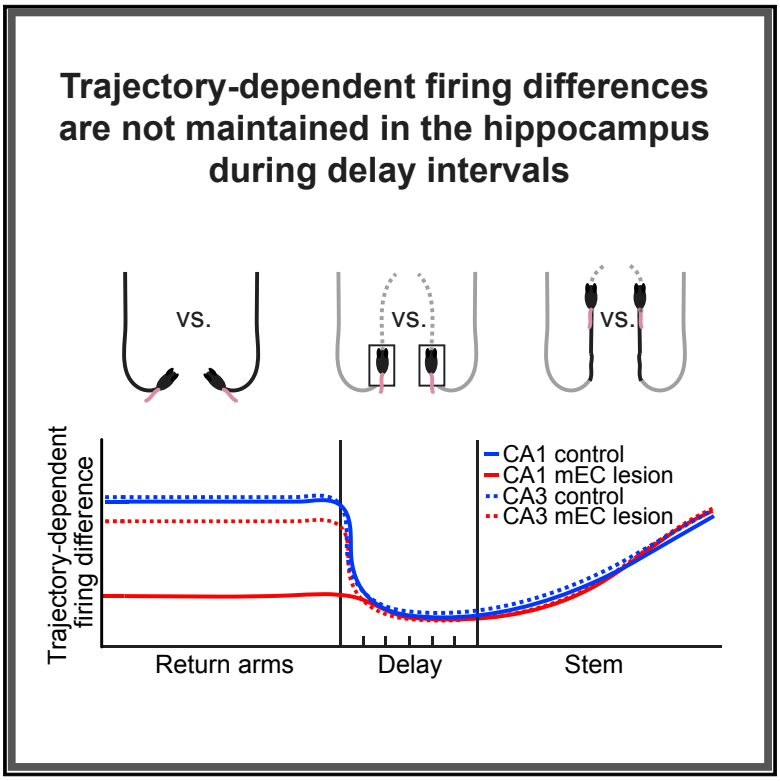

Authors

Marta Sabariego, Antonia Schönwald, Brittney L. Boublil, ..., Robert E. Clark, Jill K. Leutgeb, Stefan Leutgeb

Correspondence

sleutgeb@ucsd.edu

In Brief

Sabariego et al. provide evidence that mEC is required for working memory but not by sustaining hippocampal time cell activity during delay periods. Rather, loss of mEC inputs decreased the differential hippocampal coding between spatial locations during the encoding phase of a working memory task.

Highlights

- Neuron loss in the mEC results in an impairment in the delayed alternation task
- Hippocampal sequential cell activity during delay intervals is not required for WM
- CA1 spatial discrimination during WM encoding is disrupted by mEC lesions
- CA3 cells distinguish contexts despite the loss of mEC inputs

Sabariego et al., 2019, Neuron *102*, 1–14
June 19, 2019
https://doi.org/10.1016/j.neuron.2019.04.005

CellPress

Neuron
Article

Time Cells in the Hippocampus Are Neither Dependent on Medial Entorhinal Cortex Inputs nor Necessary for Spatial Working Memory

Marta Sabariego,[1] Antonia Schönwald,[1] Brittney L. Boublil,[1] David T. Zimmerman,[1] Siavash Ahmadi,[1] Nailea Gonzalez,[1] Christian Leibold,[2,3] Robert E. Clark,[4,5] Jill K. Leutgeb,[1] and Stefan Leutgeb[1,6,7,*]
[1]Neurobiology Section and Center for Neural Circuits and Behavior, Division of Biological Sciences, University of California, San Diego, La Jolla, CA 92093, USA
[2]Department Biology II, Ludwig-Maximilians-Universität München, Martinsried, Germany
[3]Bernstein Center for Computational Neuroscience Munich, Martinsried, Germany
[4]Veterans Affairs San Diego Healthcare System, San Diego, CA 92161, USA
[5]Department of Psychiatry, University of California, San Diego, La Jolla, CA, 92093, USA
[6]Kavli Institute for Brain and Mind, University of California, San Diego, La Jolla, CA 92093, USA
[7]Lead Contact
*Correspondence: sleutgeb@ucsd.edu
https://doi.org/10.1016/j.neuron.2019.04.005

SUMMARY

A key function of the hippocampus and entorhinal cortex is to bridge events that are discontinuous in time, and it has been proposed that medial entorhinal cortex (mEC) supports memory retention by sustaining the sequential activity of hippocampal time cells. Therefore, we recorded hippocampal neuronal activity during spatial working memory and asked whether time cells depend on mEC inputs. Working memory was impaired in rats with mEC lesions, but the occurrence of time cells and of trajectory-coding cells in the stem did not differ from controls. Rather, the main effect of mEC lesions was an extensive spatial coding deficit of CA1 cells, which included inconsistency over time and reduced firing differences between positions on the maze. Therefore, mEC is critical for providing stable and distinct spatial information to hippocampus, while working memory (WM) maintenance is likely supported either by local synaptic plasticity in hippocampus or by activity patterns elsewhere in the brain.

INTRODUCTION

Memory systems can hold previously presented information online over retention intervals of many seconds by persistent neuronal activity over temporal gaps. Although such ongoing activity was originally conceptualized as consisting of single cells that remain active over the entire delay interval (Fuster and Alexander, 1971), subsequent work has shown that persistent representations for retaining items in working memory (WM) can also be achieved with time-varying activity (Druckmann and Chklovskii, 2012). One such activity pattern consists of individual cells turning on and off at particular times within the sequence, and such cells have been referred to as time cells or sequence cells and have been described in the hippocampus (Allen et al., 2016; Gill et al., 2011; MacDonald et al., 2011; Pastalkova et al., 2008), medial entorhinal cortex (mEC) (Heys and Dombeck, 2018; Kitamura et al., 2015; Kraus et al., 2015), and prefrontal cortex (Baeg et al., 2003; Fujisawa et al., 2008; Liu et al., 2014; Tiganj et al., 2017; Yang et al., 2014). Furthermore, a major contribution of entorhinal cortex to bridging episodes separated in time is also supported by the finding that the mEC is critical for tasks with pronounced temporal components, including trace fear conditioning (Hales et al., 2018; Suh et al., 2011) and delayed matching to sample (Robinson et al., 2017). In particular, the most direct link between entorhinal contributions to hippocampal temporal firing patterns and memory performance has been reported for transient optogenetic inactivation of mEC during the delay period of a WM task, which resulted in a disruption of CA1 time cells and in memory impairment (Robinson et al., 2017).

Despite the finding that time cells are found in the entorhinal cortex and hippocampus and that inputs from the entorhinal cortex are required for temporal organization of hippocampal activity (Robinson et al., 2017; Schlesiger et al., 2015), evidence for a direct support of memory over delays by the sequential activity of time cells has remained scarce. For example, in the study by Robinson et al. (2017), memory performance partially returned to baseline during control trials after inactivation, while time cells in CA1 did not revert to the temporally organized firing during the same trials. These results were interpreted as implying that mEC manipulations caused persistent changes in synaptic organization that altered neuronal firing patterns over minutes rather than seconds, which is consistent with the finding that hippocampal spatial firing patterns in CA1 were also persistently altered after transient mEC inactivation (Rueckemann et al., 2016). Furthermore, hippocampal time cells occur without any memory demand (Salz et al., 2016), sequence discrimination can occur without differential hippocampal activity in a repeated segment (Bower et al., 2005), and differential firing on common

maze segments (i.e., trajectory coding) is more pronounced in tasks that do not depend on the hippocampus compared to hippocampus-dependent tasks (Ainge et al., 2007; Griffin et al., 2007). A further conceptual consideration is also that the continuation of sequential neuronal activation is likely time-limited by noise and thus not a mechanism that can support WM over extended delay intervals.

An alternate possibility by which the entorhinal cortex and hippocampus could support WM is by providing distinct neuronal activity patterns during the task phase when sensory inputs for the current context of the trial are available (Shapiro and Eichenbaum, 1999). The differential activity during presentation of the cues could then be maintained by synaptic plasticity in local networks over the delay interval or be informative for other brain networks that support WM. In spatial alternation tasks, differential activity in advance of the delay period in each trial would occur on the return arms. Therefore, to distinguish whether mEC inputs to hippocampus contribute to WM by discriminating the spatial context or to the maintenance of sequential hippocampal firing patterns on common maze segments, we recorded single units and local field potentials (LFPs) from the CA1 and CA3 area during a spatial alternation task in control and mEC-lesioned rats. To comprehensively identify possible mechanisms for memory maintenance over the retention interval, we tested a delay period of 10 s, over which time cells have been reported to bridge events, and a delay period of 60 s, which was chosen to identify circuit mechanisms when the capacity of ongoing sequential activity is likely exceeded.

RESULTS

Spatial WM Was mEC Dependent and Improved with Training in mEC-Lesioned Rats

The mEC is a hub that provides spatial and temporal information to the hippocampus (Hafting et al., 2005; Schlesiger et al., 2015). Therefore, we reasoned that a delayed-spatial-alternation task, which requires spatial memory retention over time and depends on hippocampal function (Ainge et al., 2007), likely also depends on mEC function. To confirm a critical role of mEC, we performed mEC lesions and trained animals to perform an alternation task on a figure-eight maze (Figures 1A and S3A). In the alternation task, rats ran down a center arm and turned left or right before returning to the base of the stem, where they were delayed for either 10 s or 60 s, or as a control, continued without a delay. On the next trial, they had to choose to turn in the opposite direction from the one during the previous trial to receive a reward. As reported for rats with hippocampal lesions in a similar task (Ainge et al., 2007), mEC-lesioned rats (n = 7) were not impaired in the continuous version of the task. While mEC- lesioned rats performed worse than controls (n = 8) with 10-s delays only at the end of the testing phase ($p = 0.010$, Tukey's test) they made significantly more errors than controls throughout all the testing phases with 60-s delays ($p = 0.0002$, 0.0013 and 0.0037, Tukey's tests) (Figure 1B and Table S1). However, WM performance significantly improved with training in both mEC-lesioned and control rats (Figure S3B), plateauing for mEC-lesioned rats well above chance levels in both the 10-s and 60-s delay conditions ($p = 0.0001$ and 0.0124, respectively, one-sample t test; Figure S3B). Our results show that mEC lesions resulted in a WM impairment, but also in partially spared memory, in particular in shorter delay conditions.

Combined Lesions of the Hippocampus and mEC Resulted in a More Severe and Long-Lasting Memory Deficit than Lesions of Only mEC

Manipulations of mEC by lesion and inactivation have previously been shown to result in substantially deteriorated hippocampal spatial and temporal firing patterns (Hales et al., 2014; Miao et al., 2015; Robinson et al., 2017; Schlesiger et al., 2015), which raises the possibility that mEC lesions result in a loss of memory-related function of not only mEC, but via the loss of mEC inputs, also of the hippocampus. If this were the case, the retained WM in mEC lesioned rats could be mediated by brain areas other than mEC and hippocampus. However, if remaining hippocampal function in mEC lesioned rats continues to at least partially support WM, hippocampal damage in addition to mEC damage should further exacerbate memory impairment. To distinguish between these possibilities, we performed combined mEC and hippocampus (mEC+H) lesions. These animals (n = 5) performed similarly to the control and mEC lesion groups during trials with no delay, consistent with the notion that neither the hippocampus (Ainge et al., 2007) nor mEC is critical for the continuous version of the task. However, with delays of either 10 s or 60 s, mEC+H lesions resulted in a much more pronounced memory impairment than mEC lesions ($p < 0.0001$, Tukey's tests; Figure 1B and Table S1). Moreover, no recovery was observed with mEC+H lesions, such that animals with combined lesions always performed at or below chance levels in both delay conditions (n.s., one-sample t tests) (Figures 1B and S3). To examine how the performance of rats with the mEC+H lesion could be below chance level, we analyzed whether these rats were prone to making strings of consecutive errors (Figure 1C). Such behavioral inflexibility was increased in rats with mEC+H lesions at longer delays ($p = 0.0002$, Tukey's test) but not in either control or mEC lesioned rats. Taken together with the results from rats with selective mEC lesions, the results from the mEC+H lesions suggest that the hippocampus, when intact in an mEC-lesioned rat, can at least partially support spatial WM.

The mEC Lesion Extent Was Similar in Rats with Only mEC Lesions and in Rats with mEC+H Lesions

To confirm that differences in performance between rats with selective mEC lesions and those with mEC+H lesions were a consequence of adding the hippocampal lesion and did not result from different lesion extents within mEC, we visualized any remaining neurons in the target of the lesion in cresyl-violet-stained sagittal sections and used the Cavalieri method to quantify the lesion extent (Figures 1D, S1A–S1C, and S2). In the mEC lesion group (n = 10), 93.0% of the total mEC volume was completely ablated (95.3% of layer II, 92.4% of layer III, and 91.4% of deep layers) with the majority of the sparing in the most ventromedial extent of the mEC (Figures 1D and S1A), which projects predominantly to the ventral hippocampus (Hargreaves et al., 2005). The lesions were extensive and consistently included the complete dorsocaudal portion of mEC where

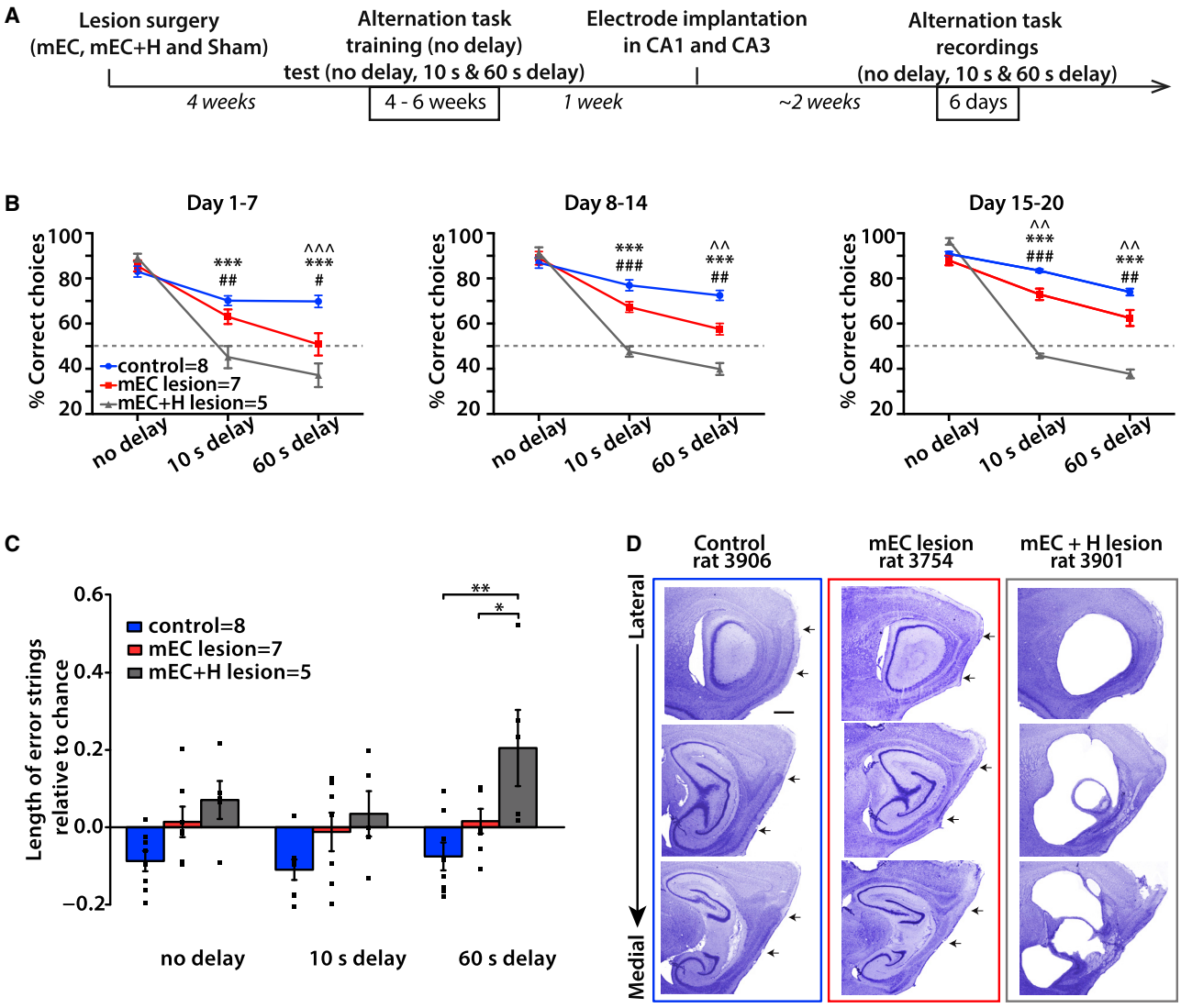

Figure 1. WM Performance Was Impaired in mEC Lesioned Rats

(A) Experimental timeline. Rats underwent mEC lesions, combined mEC+H lesions, or sham surgeries (control) and were then trained in a spatial alternation task, first with only no delay trials and later with blocks of 10-s and 60-s delay trials included on each day. Tetrodes were implanted after 14 days of behavioral training with all delay conditions, and at least 6 days of recordings in the WM task were performed after tetrodes were positioned in CA1 and CA3.

(B) Behavioral performance in the alternation task. MEC-lesioned and mEC+H-lesioned rats were impaired in the delayed versions but not in the continuous version of the task. The 20 days of testing were analyzed in three blocks (7 days, 7 days, and 6 days). Two-way ANOVAs (Group × Delay) for each of the three blocks revealed main effects of Lesion and Delay and a Delay × Lesion interaction (see Table S1). Tukey's posthoc tests: ^^ $p < 0.01$, ^^^ $p < 0.001$ for control versus mEC lesion group comparisons; ***$p < 0.001$ for control versus mEC+H lesion group comparisons; and # $p < 0.05$, ## $p < 0.01$, ### $p < 0.001$ for mEC versus mEC+H lesion group comparisons.

(C) Length of error strings relative to chance. Given the number of errors committed by the animals in each group and condition, the average number of consecutive errors that would be expected by chance was calculated by shuffling these data 100 times and by then subtracting the shuffled values from the average number of consecutive errors observed. A two-way ANOVA (Group × Delay) revealed a significant effect of Group ($p = 0.0029$), and the differences between groups were in the 60-s delay condition where the combined lesion group made significantly more consecutive errors than both the control group and the mEC lesion group (**$p = 0.0002$ and *$p = 0.019$, Tukey's test).

(D) Series of sagittal sections from a control (left), an mEC-lesioned (middle), and an mEC+H lesioned (right) rat.

Scale bar, 500 μm. Arrows indicate the dorsal and ventral borders of mEC. Symbols and error bars in B and C are the mean ± SEM. See also Figures S1, S2, and S3 and Tables S1 and S3.

grid cells and other spatially selective cells are found (Diehl et al., 2017; Hafting et al., 2005). In the group with mEC+H lesions, 93.8% of the total mEC volume was completely ablated (91.3% of layer II, 95.0% of layer III, and 95.1% of deep layers), again with the majority of sparing in the most ventromedial extent of the mEC. No significant differences in mEC lesion extent were

found between the mEC lesion and mEC+H lesion group (n.s., two-way ANOVA with control/lesion groups and brain areas as factors). Damage to areas other than mEC was predominantly observed in parasubiculum (Figures S1C and S2B and Table S3). In the mEC+H lesion group, hippocampal lesions were extensive and included all subregions and a substantial portion of the presubiculum (94.9% of CA areas, 92.9% of DG, 90.0% of subiculum, and 78.9% of presubiculum; see Figure S2).

Hippocampal Spatial Firing Patterns in the Alternation Task Were More Severely Disrupted in the CA1 Compared to the CA3 Subregion

The finding that mEC+H lesions resulted in a much more severe memory impairment than lesions of only the mEC suggests that the hippocampus contributes to spatial memory after loss of mEC inputs. To identify hippocampal network mechanisms that could support the retained spatial WM, we compared the firing patterns of CA1 cells between control rats and mEC-lesioned rats while rats performed the spatial alternation task. Because spatial deficits in CA1 after mEC lesions were previously reported to be substantial (Hales et al., 2014; Miller and Best, 1980; Schlesiger et al., 2015), we also examined whether CA3 spatial firing patterns depended on mEC inputs to the same extent as CA1 (n = 246 CA1 and 218 CA3 cells in 7 control rats; 233 CA1 and 359 CA3 cells in 10 mEC-lesioned rats).

We began our analysis by asking to what extent the hippocampal code for space was preserved across the entire figure-eight maze while lesioned rats performed the alternation task. For this analysis, we selected cells with a peak rate of >2 Hz in at least one spatial bin, which included 72.4% and 67.8% of CA1 principal cells and 44.0% and 39.8% of CA3 principal cells in the control group and mEC lesion group, respectively. First, we evaluated whether the loss of inputs from mEC to hippocampus resulted in changes of average and peak firing rates but did not find differences for either measurement in CA1 or CA3 (n.s., KS test; Figure 2B). Next, we compared the spatial information of place fields between groups. Firing fields of CA1 pyramidal cells in the mEC lesion group had less spatial information compared to control CA1 cells ($p < 0.0001$, KS test; Figures 2A and 2B). In contrast, CA3 pyramidal cells of mEC-lesioned rats did not differ from CA3 control cells and CA1 control cells (n.s., KS tests). Consistent with the pronounced effect of the lesion on spatial information in CA1, CA1 place fields were larger in mEC lesioned rats compared to CA1 controls ($p < 0.0001$, KS tests; Figure 2B). While CA3 field size was also moderately increased in mEC-lesioned compared to control rats, the increase was less than in CA1 ($p < 0.0001$, two-way ANOVA; Figure 2B).

The hippocampal code for space could support spatial memory not only by firing at well-defined locations, but also by reliably firing at particular places. To examine the consistency of firing patterns between trials, we computed correlation coefficients between the spatial firing patterns of each trial with the spatial firing patterns of all other trials of the same type (i.e., between all pairs of right-turn trials and between all pairs of left-turn trials) and averaged these values. No differences in spatial stability between control CA1 and control CA3 cells were found (n.s., KS test), while CA1 and CA3 cells from mEC-lesioned rats fired less consistently at the same location than those from control rats ($p < 0.0001$, KS test). However, mEC lesions had a more minor effect on the trial-by-trial correlations of CA3 cells compared to CA1 cells ($p < 0.0001$, two-way ANOVA; Figure 2B).

Spatial Discrimination between Return Arms Was More Severely Disrupted in CA1 Compared to CA3

In spatial alternation, a subsequent correct choice depends on the accurate encoding of the preceding trajectory. Distinct representations of right- and left-return arms could be particularly relevant to task performance. To measure the difference in firing patterns between one compared to the other side of the maze, we computed the spatial correlation between corresponding positions on the left versus right side of the maze (previously referred as "path equivalency"; Singer et al., 2010). To exclude effects from taking different turns at the choice point, we focused only on correct choices. We found higher correlation coefficients for CA1 cells of mEC-lesioned compared to control rats ($p < 0.0001$, KS test), which indicated that cells in lesioned rats were more likely to fire at corresponding locations and showed reduced separation between left and right trajectories during the alternation task. In contrast, most active CA1 cells in return arms of control rats fired almost exclusively on only one side of the maze (Figure 3A). To confirm that the increased path equivalency in mEC-lesioned rats could not emerge by firing patterns overlapping by chance for cells with broader spatial firing in the maze, we performed shuffling of the right and left maze segments with respect to one another and obtained correlation coefficients from shuffled data that were substantially below the observed ones (all $p < 0.0001$, KS tests, Figure S4).

Given that task-relevant information in the hippocampal CA1 area was substantially reduced in the return arms of mEC lesioned rats but that the hippocampus could nonetheless continue to partially support WM, we sought to identify whether hippocampal firing patterns remained intact in CA3. Consistent with the more minor effect on CA3 spatial coding when analyzing the entire maze (see Figure 2B), CA3 cells of mEC lesioned rats were also found to fire more exclusively on only one side of the maze and thus distinguished readily between left and right, similar to the pattern observed for control cells (Figure 3B).

Time Cells during the 10-s Delay Period in Control and mEC-Lesioned Rats Did not Distinguish between Left-Turn and Right-Turn Trials

WM tasks have previously been found to display sequential neuronal activity during the delay period that discriminated between trial types. However, such activity was predominantly reported in an object-odor association task (MacDonald et al., 2011; Robinson et al., 2017) and in an alternation task that required continuous running during the delay period (Pastalkova et al., 2008). In our version of the task, animals were not forced to run during the delay and were tested with delay intervals of 10 s and 60 s. Without the requirement to continuously run in the alternation task, we found that only a low proportion of hippocampal CA1 and CA3 cells was active during the delay

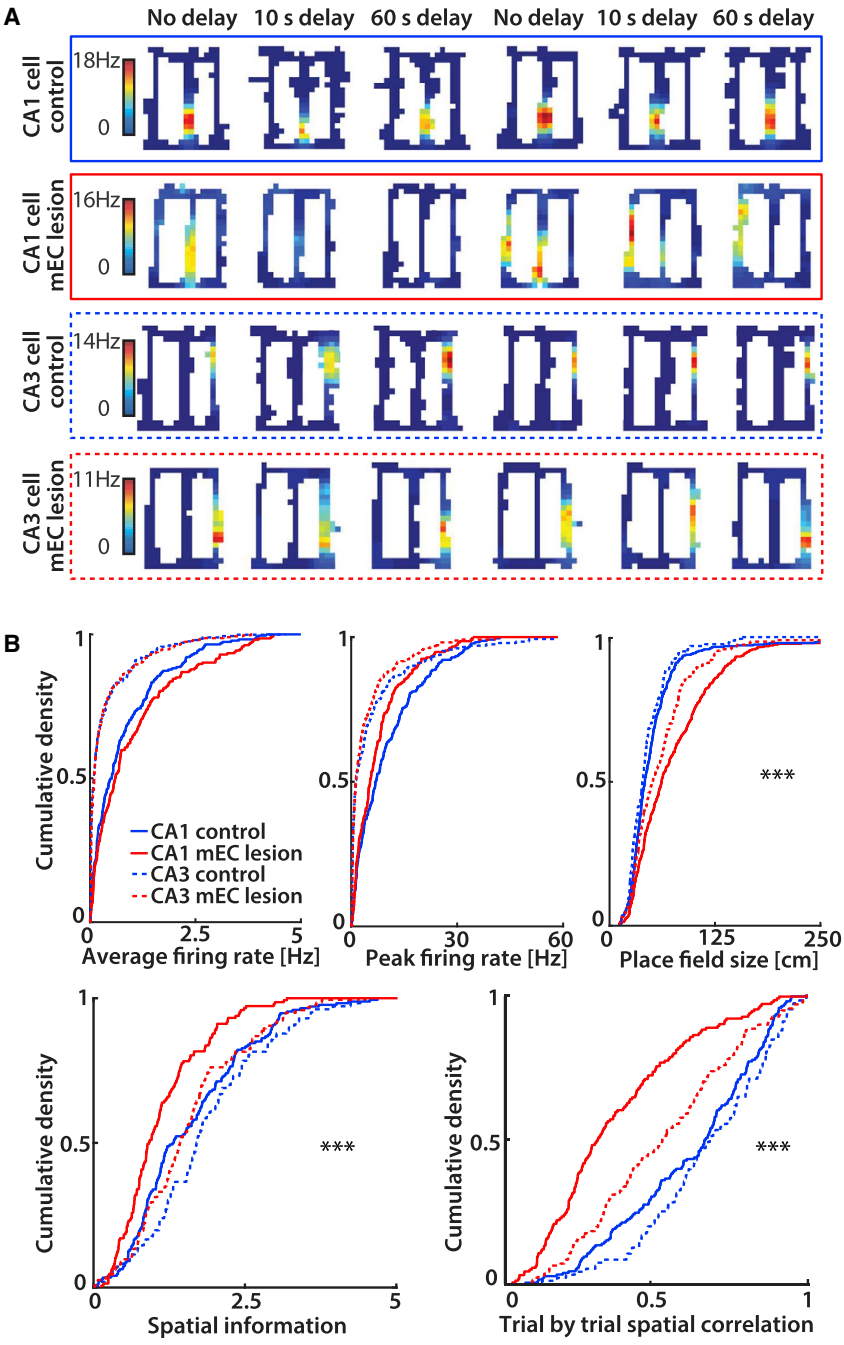

Figure 2. MEC Lesions Had a Larger Effect on Field Size, Spatial Precision, and Stability in CA1 Compared to CA3

(A) Rate maps of CA1 and CA3 cells. Each row is a cell's firing pattern for each of the 6 blocks (two per delay condition). CA1 place fields were unstable and changed firing location in mEC-lesioned rats. Color bars indicate the firing rate (from 0 Hz in blue to the peak rate in all blocks in red).

(B) Cumulative density functions (CDFs) of average firing rate, peak firing rate, field size, spatial information, and trial-by-trial spatial correlation. Average firing rates and peak firing rates were not different between control and mEC lesion groups in either CA1 (mEC n = 233 cells, control n = 246 cells; n.s., KS test) or CA3 (mEC n = 359 cells, control n = 218 cells; n.s., KS test). CA1 and CA3 place fields were larger in the mEC lesion group compared to controls ($p < 0.0001$, KS test) with a larger effect on CA1 than CA3 place field size in mEC lesioned rats (two-way ANOVA with Lesion × Hippocampal subfield as factors; posthoc analysis, Tukey's test: differences between CA1 and CA3 in the control group, n.s., in the mEC lesion group, ***$p < 0.0001$). Spatial information for cells active on the maze (peak firing >2 Hz) was different between control and mEC lesion groups in CA1 (mEC n = 158 cells, control n = 178 cells; ***$p < 0.0001$, KS test), but not CA3 (n = 143 cells, control n = 96 cells; n.s., KS test). Trial-by-trial spatial correlation (i.e., spatial stability) for cells active on the maze was lower in the mEC lesion compared to the control group in both CA1 and CA3 (***$p < 0.0001$, KS tests). The effect on spatial stability was larger in CA1 compared to CA3 in mEC-lesioned rats (two-way ANOVA with Lesion and Hippocampal subfield as factors; posthoc analysis, Tukey's test: spatial stability differed between every combination of subfield and lesion, all p values < 0.001, except between control CA1 and control CA3).

See also Figure S1.

period in control as well as mEC-lesioned rats (Figures 4A and 5A). Because neuronal firing patterns that are informative about trial type should be most pronounced during correct trials, we focused on correct trials for our analyses. Despite the small proportion of active cells during the delay, we found that the firing patterns were sequentially organized over the 10-s delay, as previously reported for delay periods of similar length (MacDonald et al., 2011; Pastalkova et al., 2008; Robinson et al., 2017). However, the sequential firing patterns were not any more distinct between left-turn and right-turn trials than between blocks of trials of the same type, and sequential firing patterns were not deteriorated in animals with mEC lesions (n.s., two-way ANOVA with trial type and control/lesion group as factors; Figures 4B and 4C). Consistent with the uninformative left-right differences in sequential activity, we found that there were no trial-type-dependent rate differences when averaging firing rates over either the first 5 s or the second 5 s (all Mann-Whitney tests against shuffled values, n.s., Figure 4C).

Discontinuous Events over Longer Retention Intervals Were Not Bridged by Time Cells

Previous studies that reported time cells used delays of up to 20 s (MacDonald et al., 2011; Pastalkova et al., 2008), but it is well established that hippocampus-dependent memories can be retained for longer time periods. Analysis of firing patterns during the 60-s delay afforded us the opportunity to test whether

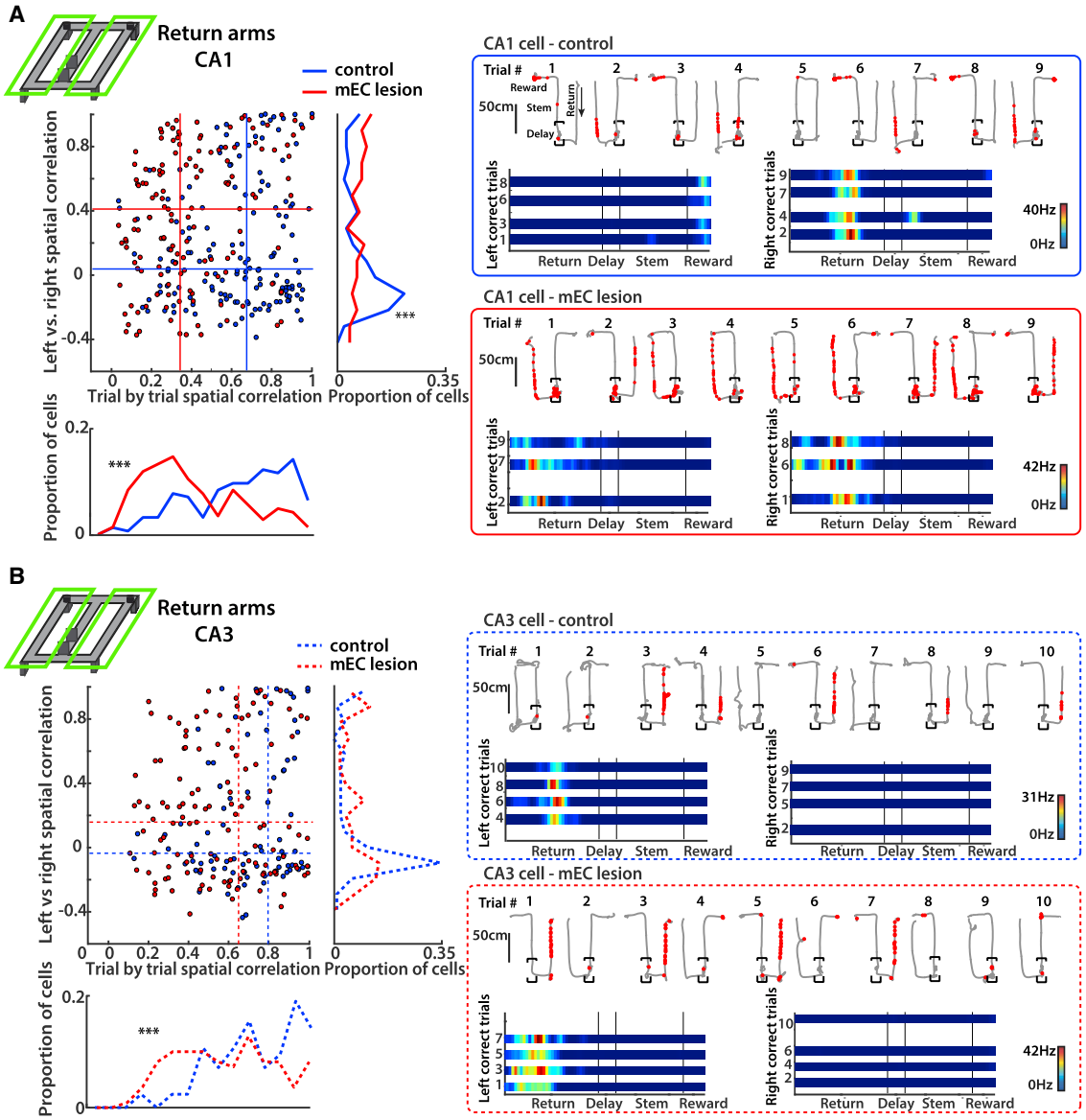

Figure 3. MEC Lesions Impaired Spatial Coding on the Return Arms to a Larger Extent in CA1 than in CA3

(A) (Left) Spatial correlation between the average firing pattern on left compared to right maze segments (left versus right, vertical axis) and, as a measure of place field stability, between single trials with the same turn direction (trial-by-trial, horizontal axis). Only correct trials were used for the analysis, and each dot in the scatterplot is a CA1 cell. Data for each type of spatial correlation are summarized in histograms to the right and on the bottom (***$p < 0.0001$, KS test). The median values of each group (control and mEC lesion) are shown as horizontal and vertical lines within the scatterplot. (Right) Example CA1 cells from a control and an mEC-lesioned rat. Top row of each example are single correct and incorrect trials (path in gray, spike locations as red dots), and bottom row are linearized rate maps of correct left and correct right trials. Color bars indicate the firing rate (from 0 Hz in blue to the peak rate in all trials in red).

(B) Same as (A), but for CA3 cells. A larger number of CA3 compared to CA1 cells in mEC-lesioned rats were stable from trial to trial and discriminated between right and left maze segments.

See also Figure S4.

sequential activity patterns in the hippocampus are also the mechanism that is used over delay intervals that are longer than tested in previous studies of sequence activity. In 60-s delays, we found that neuronal activity patterns showed evidence for sequence coding during the initial few seconds (Figure 5B). However, omitting the first 10 s from the analysis of time bin correlations revealed that hippocampal firing patterns were no longer temporally organized for the remaining 50 s (Figure 5C insets), and these results did not differ between the control and mEC-lesion group (n.s., two-way ANOVA tests). Furthermore, we confirmed with additional analyses that the firing patterns of cells over the delay interval were not informative about the trajectory. First, by computing correlations for sequences within each 5-s interval we confirmed that sequential cell activity was either not

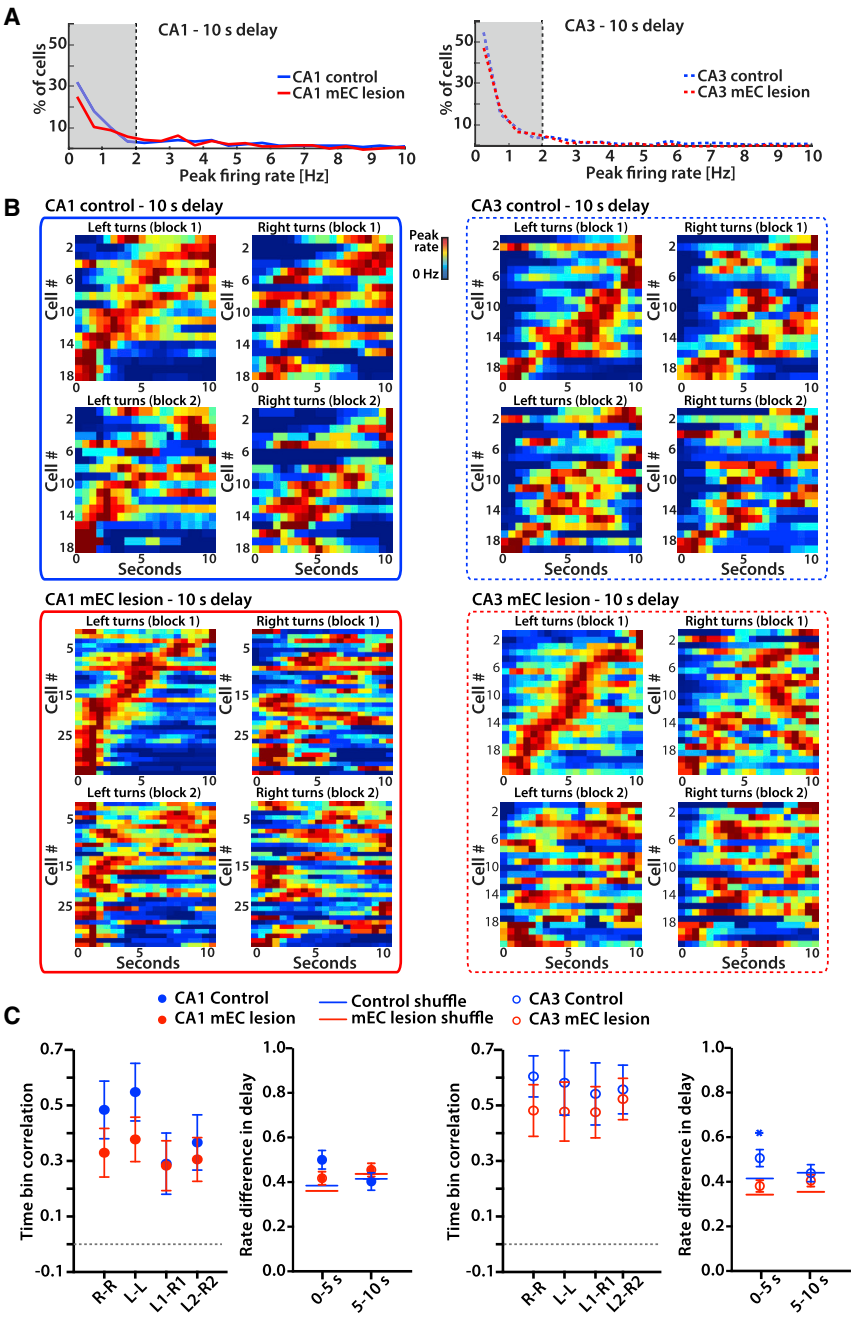

Figure 4. Time Cells during the 10-s Delay Period Did Not Distinguish between Left-Turn and Right-Turn Trials in Either Control or mEC-Lesioned Rats

(A) For each cell, firing rates were calculated for 500-ms bins throughout the 10-s delay interval of correct trials. The distribution of peak firing rates from all CA1 cells (left) and CA3 cells (right) from control and mEC lesioned rats is shown. Cells with peak rates >2 Hz in at least one time bin were considered active during the delay.

(B) Temporal firing patterns of all CA1 cells and CA3 cells that were active during the 10-s delay. Each row is the average firing rate for a single cell over one block, normalized to the cell's peak rate. Cells are sorted by the time of the peak during the first block of left-turn trials. Color bars indicate the firing rate from 0 Hz in blue to the peak rate in red.

(C) For each cell, the correlation between corresponding time bins over the 10-s delay (i.e., time bin correlation) was calculated between left-turn and right-turn trials within a block and between trials of the same type across the two blocks (n.s., two-way ANOVA with trial type and blocks as factors).

Symbols and error bars are the mean ± SEM. Left versus right rate differences in delay were also calculated using 5 s increments (*$p < 0.05$, Mann-Whitney test). See also Figure S5 and Table S4.

observed or when observed (e.g., during the initial 5-s period) did not differentiate between left versus right trials (Figures S5A and S5B and Table S4 for statistics). Second, we constructed population vectors in time intervals of 1-s span and trained a linear classifier to distinguish left and right turns based on the population activity (Figure 6A). The classifier was not able to detect trial type for either future or past trajectories in CA1 and only to a very minor extent in CA3 (Figure 6A). Finally, we compared firing rate differences for each 5-s segment of the delay interval between trial types and found that differences were only higher than for shuffled data during the first 5 s of the delay, but not for the remainder of the delay interval (Figure 6B). Neither sequential nor differential neuronal activity in the hippocampus was therefore observed for memory retention over the longer delay interval in either control or mEC-lesioned rats, and the population activity was not informative for decoding trial type.

Similarity of Hippocampal Activity during the 10-s Delay and the First 10 s of the 60-s Retention Interval

Because we found evidence for sequential activity during the 10-s delay as well as over the first seconds in the 60-s delay, we tested whether these sequences were corresponding. A comparison between the sequences across the two different delays revealed that sequences within the 10-s delay were highly correlated to sequences over the first 10 s of the 60-s delay for CA1 cells as well as CA3 cells (Figure S5C). Correspondingly, we also found that most cells that were active during the 10-s delay were also active over the first 10 s of the 60-s delay (Figure S5D). Although our data revealed matching activity over the first 10 s of absolute time, it has also been reported that the duration of hippocampal firing can expand or compress, such that the periods when cells fire remain at corresponding relative timepoints within each interval (MacDonald et al., 2011). However, our analysis revealed substantially lower correspondence with relative compared to absolute time (all $p < 0.001$, Mann-Whitney tests,

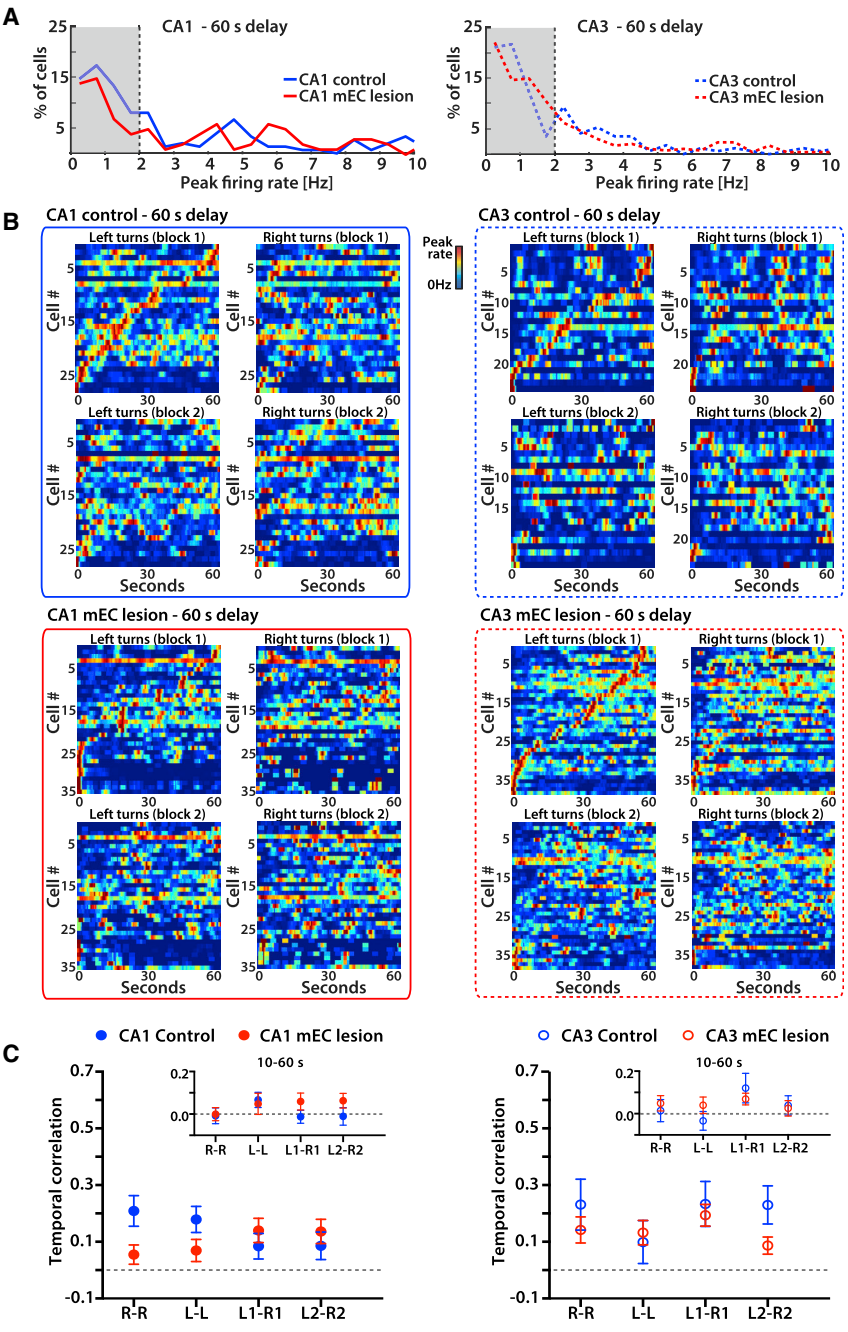

Figure 5. Time Cells Do Not Bridge Discontinuous Events over 60-s Retention Intervals

(A) For each cell, firing rates were calculated for each 500-ms bin throughout the 60-s delay interval of correct trials, and the distribution of peak firing rates from all CA1 (left) and CA3 (right) cells from control and mEC lesioned rats is shown.

(B) Temporal firing patterns of all CA1 cells and CA3 cells that were active during the 60-s delay. Each row is the average firing rate for a single cell over one block, normalized by the cell's peak rate. Cells are sorted by the time of the peak during the first block of left-turn trials. Color bars indicate the firing rate from 0 Hz in blue to the peak rate in red.

(C) For each cell, the correlation between corresponding time bins over the 60-s delay (i.e., temporal correlation) was calculated between left-turn trials and between right-turn trials within a block and between trials of the same type across the two blocks (n.s., two-way ANOVA with Trial type and Blocks as factors). Symbols and error bars are the mean ± SEM. Insets: cell-by-cell temporal correlation between blocks and trial types, excluding the first 10 s of the 60-s delay interval (n.s., two-way ANOVA). See also Figures S5 and S6 and Table S4.

Figure S5C), consistent with our results that there are no detectable timed patterns after the initial 10 s in the 60-s delay.

Hippocampal Cells that Are Active during the Delay Are Partially Corresponding to Cells that Are Active in Other Maze Segments

It has recently been reported that mEC time cells that are active during immobility form a subpopulation that is distinct from mEC cells that are spatially modulated (Heys and Dombeck, 2018). Therefore, we tested whether hippocampal cells that were active when rats stopped during the delay were distinct from those that were active while running in other maze segments. In contrast to mEC cells, the fraction of CA1 and CA3 cells that were active during the delay as well as elsewhere on the maze was higher than expected (all p values < 0.01, chi-square tests, Figure S6). The same result was obtained even after further restricting the firing rates to periods of immobility by omitting the first 5 s in the delay, which is the period when rats had not yet slowed down. Again, more cells than expected were active in both the delay and elsewhere (all p values < 0.001, chi-square tests).

Trajectory-Dependent Firing Differences in the Maze Stem Were Not Reduced by mEC Lesions

In addition to the delay zone, the stem is the part of the maze where animals have to retain or recall information about the previous trajectory to correctly decide on the next choice. Accordingly, hippocampal cells have been reported to fire differentially on the stem between trial types with different upcoming choices, even while the rat is in the same spatial location (Ainge et al., 2007; Bower et al., 2005; Ferbinteanu and Shapiro, 2003; Frank et al., 2000; Griffin et al., 2007; Johnson and Redish, 2007; Pfeiffer and Foster, 2013; Smith and Mizumori, 2006; Wood et al., 2000). Such trajectory-dependent differential hippocampal activity in advance of the turn could provide an internal representation that is used to support the appropriate upcoming goal choice. When analyzing differential activity of the cells that were active on the stem, we found that a large

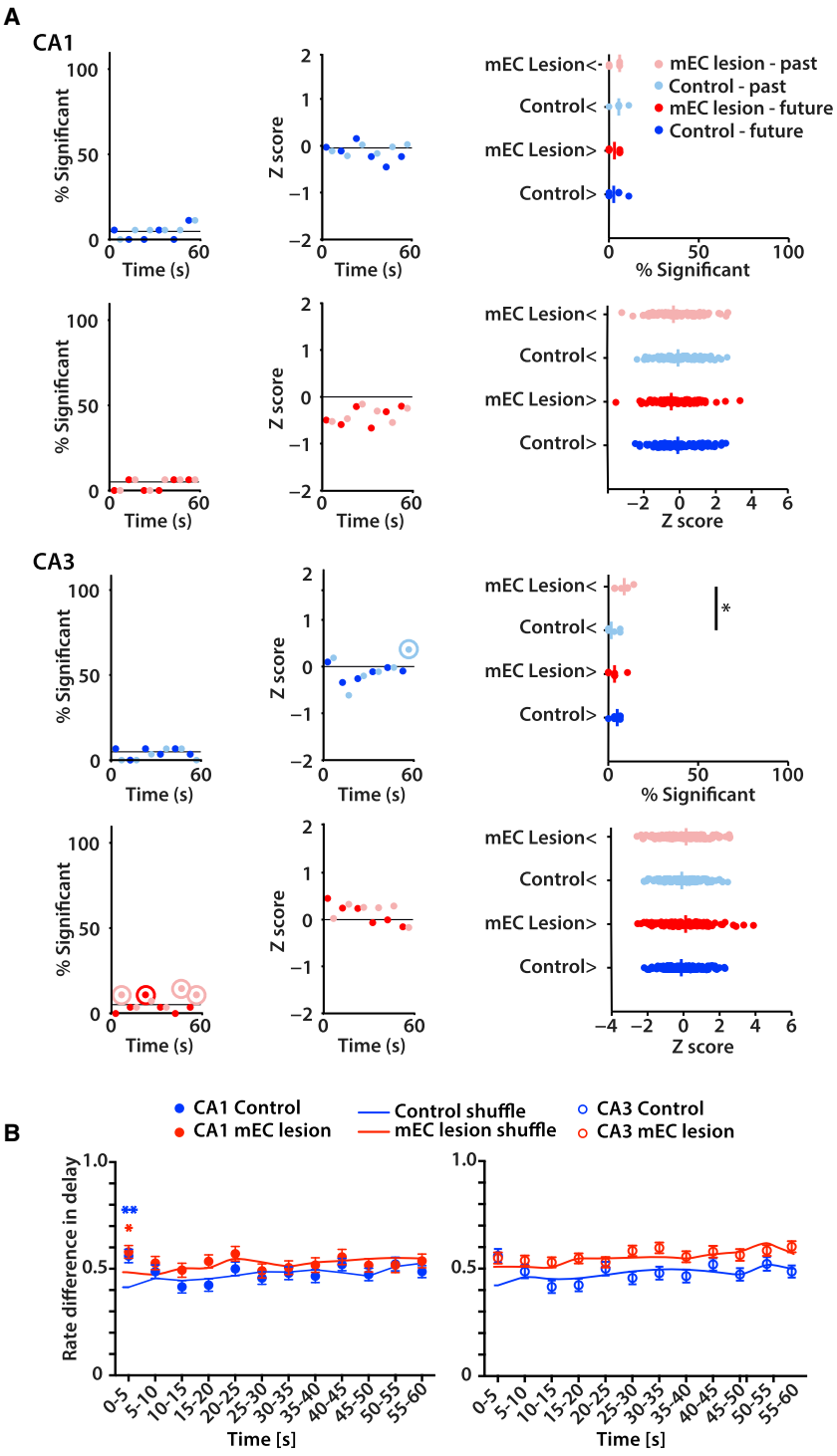

Figure 6. Trial Type Could Not Be Decoded with a Linear Classifier or from Rate Differences Past the First 5 s of the 60-s Delay

(A) (Left) Fraction of sessions in which the correct classification rate (CCR) from the real data were in the upper 95% quantile of the shuffles. Analysis was done for 1-s-long population vectors within each 10-s time segment of the 60-s delay and by using either upcoming turn direction (dark colors) or previous turn direction (light colors). Dots in circles indicate significance using a Binomial test, $p < 0.05$. (Middle) Median Z score of CCRs within each 10-s interval. Z scores were calculated by comparing real CCR values to distributions for which the trial-type label was shuffled. Dots within circles indicate significance using a Wilcoxon test, $p < 0.05$. (Right) Data from all 10-s intervals and sessions were tested for significant differences between groups (% significant, $^*p < 0.05$, Mann-Whitney test) or for differences from zero (Z scores, all n.s., Wilcoxon test).

(B) Left versus right rate differences during delay were calculated using 5-s time segments. The differences calculated from real data were compared to rate differences from data shuffled by trial type. Rate differences were only informative about trial type in CA1 during the first 5 s ($^*p < 0.05$, $^{**}p < 0.01$, Mann-Whitney test).

Symbols and error bars are the mean ± SEM

proportion of CA1 and CA3 cells in the control (CA1: 13 of 28 cells; CA3: 4 of 8 cells) and mEC lesion group (CA1: 9 of 20 cells; CA3: 10 of 15 cells) became differentially active, in particular in the most distal part, when the path of the animal started to deviate toward one side (see Figures 7 and S7 for comparison, and Table S2). In order to reduce a potential bias from the deviation of trajectories in the final segment of the stem, we excluded the last 25 cm of the stem (up to 7.1 cm deviation in the final segment, 0.50–1.49 cm deviation in the remaining segments) from our analysis and found that the number of active cells dramatically decreased in both CA1 and CA3. Accordingly, trial-type-dependent firing only consistently differed from shuffled data when including (all p values < 0.05, KS tests), but not when excluding the final segment (Figure S7C).

DISCUSSION

Although mEC and hippocampus are both known to be critical for spatial and temporal components of memory, the circuit mechanisms for the processing of space and time remain incompletely understood. To investigate how mEC contributes to memory-related hippocampal function, we compared memory deficits between rats with combined mEC and hippocampus lesions and rats with only mEC lesions. Both lesion groups performed at control levels in a spatial alternation task without a delay, which is a task version that is known not to depend on the hippocampus and can likely be accomplished as a habit (Ainge et al., 2007). In versions of the spatial alternation task that include a delay and are thus hippocampus-dependent (Aggleton et al., 1986; Ainge et al., 2007; Dudchenko et al., 2000;

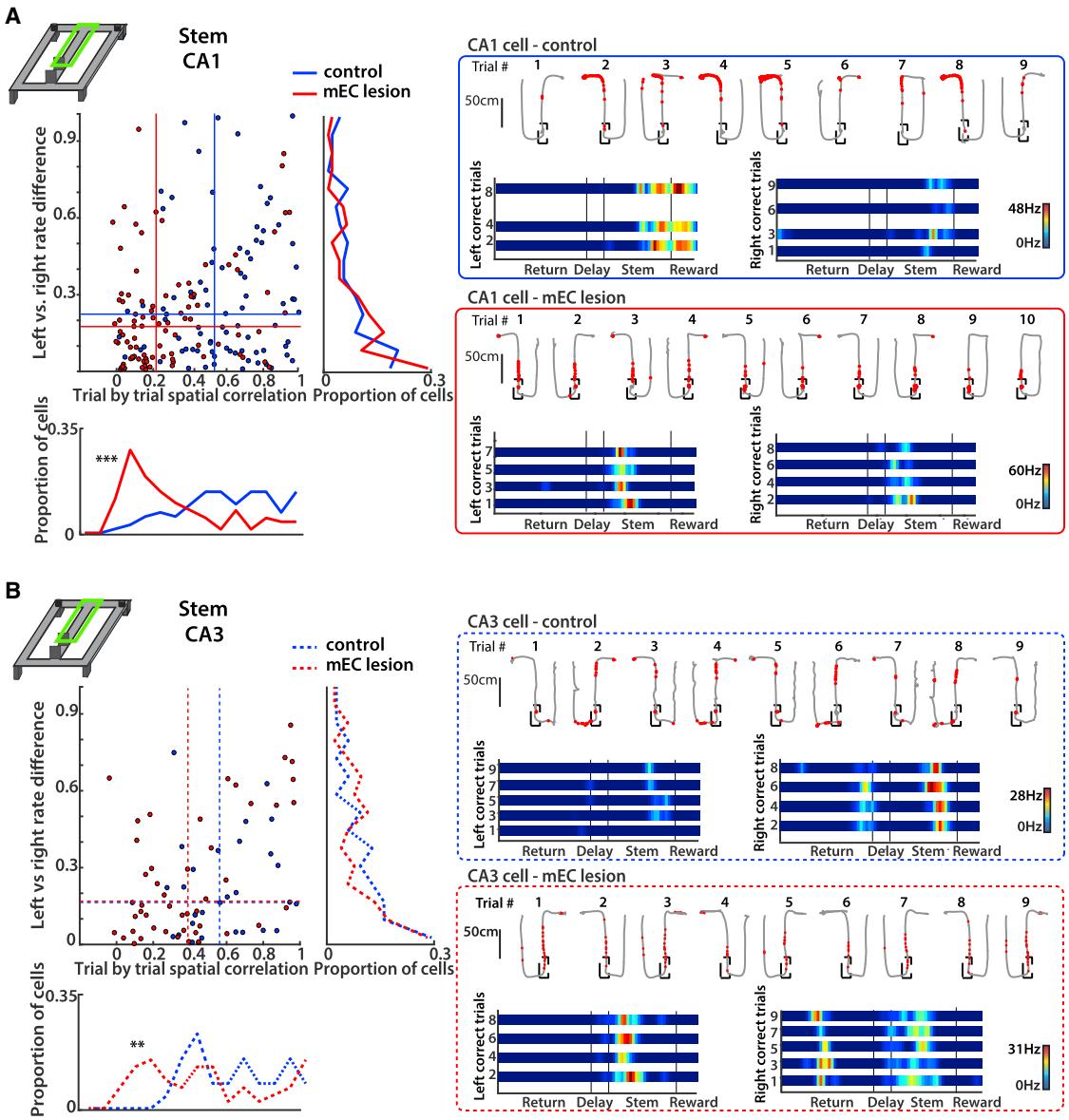

Figure 7. Trajectory-Dependent Firing in the Stem Was not Reduced by mEC Lesions for either CA1 or CA3 Cells

(A) (Left) CA1 rate differences between correct left-turn and right-turn trials (left versus right, vertical axis), and spatial correlation coefficients between single trials with the same turn direction (trial-by-trial, horizontal axis). Data for the trial-wise spatial correlations are summarized in the histogram on the bottom (trial-by-trial, ***$p < 0.0001$, KS test), and data for the rate differences are summarized to the right (left versus right rate difference, n.s., KS test). The median values of each group (control and mEC lesion) are shown as horizontal and vertical lines within the scatterplot. (Right) Example CA1 cells from a control and an mEC-lesioned rat. Top rows of each example are single correct and incorrect trials (path in gray, spike locations as red dots), and bottom rows are linearized rate maps of correct-left and correct-right trials. Color bars indicate the firing rate with 0 Hz in blue and the peak rate in all trials in red. Note that most cells with differential activity on the stem fire at corresponding locations across trials but with higher rates in one trial type compared to the other.

(B) Same as (A), but for CA3 cells. In control and MEC-lesioned rats, similar proportions of CA1 and CA3 cells show differences in firing between correct left-turn and correct right-turn trials. Trial-wise spatial correlations were decreased by the mEC lesion (bottom: **$p < 0.01$, KS test).

See also Figure S7 and Table S2.

Olton et al., 1979), rats with mEC lesions showed mild deficits in memory performance with 10-s delays and more pronounced deficits at longer delays. For both delays, memory performance was better preserved with mEC lesions than with combined mEC and hippocampus lesions. These results suggest that mEC lesions disrupt memory-related hippocampal neural activity, but that there is, in rats with only mEC lesions, nonetheless spared task-relevant spatial and temporal hippocampal activity that can support WM performance above chance. Thus, we examined hippocampal neuronal firing patterns during the memory

task and found that loss of mEC inputs substantially reduced spatial coding in CA1, but to a lesser extent in CA3. In contrast, time cells over a 10-s delay were not diminished by the mEC lesion in either the CA1 or the CA3 subregion. However, in control and lesioned rats, time cells did not show distinct firing patterns between right-turn and left-turn trajectories. With 60-s delays, we did not detect trial-type dependent activity past a period of ~10 s, which further confirmed that differences in sequential hippocampal activity could not have been informative over the delay period. However, trajectory-dependent hippocampal activity re-emerged in both control and mEC lesioned rats along the stem of the maze. Taken together, these results suggest that partial memory deficits after mEC lesions are accompanied by less informative spatial firing patterns, which could hinder the encoding and updating of information during the return to the delay zone. In contrast, hippocampal firing patterns over the delay interval were neither found to be informative for memory performance nor dependent on mEC inputs, which suggests that memory retention does not require continuously ongoing hippocampal activity during the delay interval.

While we did not find that cells in the delay zone were informative for spatial memory retention in delayed spatial alternation, previous studies that tested a potential contribution of the hippocampus and entorhinal cortex to WM have emphasized the coding properties of cells that are sequentially and differentially active during either the delay interval or on the maze stem. During these task phases, sensory information about the previous choice is no longer available, which implies that a trace of the previous experience needs to be held in memory. Thus, it has been suggested that hippocampal and entorhinal activity patterns over delay intervals are a key mechanism for maintaining the temporal continuity and for binding temporally discontinuous events (Eichenbaum, 2014; Kraus et al., 2015; MacDonald et al., 2011). Moreover, to be informative for subsequent choices, activation patterns of hippocampal cells would need to differ between trial types in WM tasks. However, such differential activity has been found to be particularly pronounced in tasks that are known to not be hippocampus-dependent or for which dependence on the hippocampus has not been explicitly tested (Ainge et al., 2007; Griffin et al., 2007; Hölscher et al., 2004; Ito et al., 2015; Lee et al., 2006; Wood et al., 2000). Paradoxically, for versions of spatial WM tasks, which are hippocampus dependent, previous reports found that hippocampal CA1 activity during the delay or initial portion of the stem was not informative about the subsequent choice (Ainge et al., 2007; Ito et al., 2015). Although the occurrence of differentially active hippocampal cells on common maze segments is well established, the necessity of such trajectory-dependent activity for memory retention in a hippocampus-dependent version is supported neither by previous findings nor by our findings.

A key difference between spatial-alternation tasks without differential activity compared to those that reported differential activity is that those with differential activity typically required running over the entire delay period of up to 15 s (Pastalkova et al., 2008). The requirement to run resulted in sustained hippocampal theta oscillations over the entire delay, which could be a prerequisite for making the sequential activity contingent on the preceding trajectory (Buzsáki and Moser, 2013). However, in numerous hippocampus-dependent tasks with delay intervals, ongoing theta states are not a prerequisite for memory retention (Ainge et al., 2007; Clark et al., 2000, 2002; de Lima et al., 2006; Duva et al., 1997; Hammond et al., 2004; Mumby et al., 1996; Prusky et al., 2004; Rampon et al., 2000; Takehara et al., 2003), which raises the question whether tasks without continuous running throughout the delay period may depend on different network mechanisms. Here, we show that, in a task in which animals are not required to run over the delay, hippocampal cells are not differentially active between left-turn and right-turn trials except during the first few seconds. This suggests that hippocampal sequential activity over time is at best critical for memory retention over short intervals and that other mechanisms likely support working memory over longer intervals and in situations when theta states are not continuous but when tasks critically depend on the hippocampus and entorhinal cortex. For example, awake sharp-wave ripples in hippocampus occur during brief periods of immobility and were found to be critical for future route planning and behavioral performance in spatial WM tasks (Girardeau et al., 2009; Jadhav et al., 2016; Sasaki et al., 2018).

In addition to observing that time cells were not informative for memory performance, we also found that time cells persisted in mEC-lesioned rats. Our results show that the specialized population of mEC time cells that is active during immobility (Heys and Dombeck, 2018) is not necessary for generating hippocampal time cell patterns during immobility over the delay interval. Furthermore, the hippocampal cells that were active during the delay were not a distinct population from those active in other parts of the maze, which is consistent with the findings that hippocampal cells can code for multiple features of a task (MacDonald et al., 2011; McKenzie et al., 2014). In addition, our finding of partially retained hippocampal time cells while memory performance is impaired appears to contradict a previous report that found CA1 time cells in an object discrimination task and that showed that sequential hippocampal activity as well as memory performance were diminished when mEC was optogenetically inhibited (Robinson et al., 2017). However, the transient mEC inactivation by Robinson et al. (2017) did not only result in a reorganization of hippocampal time cells during the period of mEC inhibition, but rather the change in hippocampal firing patterns also persisted throughout trials in which the stimulation was not applied. Despite the disrupted sequence firing in no-stimulation trials, the manipulation did not cause a significant behavioral impairment in no-stimulation compared to baseline trials. Therefore, it appears that mEC inactivation resulted in a long-lasting reorganization of hippocampal sequential firing while hippocampus-dependent WM performance could at least partially recover in the absence of time cells. The partial recovery of memory but not of time cells can be considered as further evidence that time cells are not critical for WM performance.

If the function of hippocampus is not to provide persistent activity over the delay interval, how is memory retained and how do mEC and hippocampus contribute to memory retention? Although it is feasible that persistent activity over the delay could occur elsewhere in the brain, prefrontal cortex delay activity has been reported to correlate with memory retention only during

learning but not in a well-trained WM task (e.g., Liu et al., 2014). Furthermore, in a delayed spatial alternation task, activity patterns in neither medial prefrontal cortex nor nucleus reuniens were informative about the preceding trajectory during the second half of a 10- to 15-s-long delay (Ito et al., 2015). In addition, prefrontal areas only compensated for hippocampal damage over short retention intervals (Lee and Kesner, 2003), and we show here that there is no compensation for combined mEC and hippocampus damage even with delays that are as short as 10 s. In contrast, memory partially recovered with mEC lesions, which suggests that degraded output from the hippocampus becomes progressively more useful with functional recovery or training. These findings suggest that the prefrontal cortex or other brain regions outside of the hippocampal formation can, at least partially, support task performance when at the minimum supplied with a spatial signal of low quality.

Together with previous studies (Ito et al., 2015; Lee and Kesner, 2003; Liu et al., 2014), our findings also raise the possibility that WM retention, over longer intervals in particular, may not be supported by persistent neuronal firing patterns. The encoding of a preceding trajectory would thus be more likely supported by other mechanisms, such as synaptic modifications within each trial throughout periods when cells are silent or not differentially active (Barak and Tsodyks, 2014; Ito et al., 2015; Mongillo et al., 2008; Stokes, 2015). With memory storage over the delay interval by modified synaptic connectivity, subsequent task-relevant activity would need to be reinstated, as indicated by the reemergence of trajectory-dependent activity in advance of the choice point (Figure 7; Ito et al., 2015). However, the reemergence of trajectory coding on the stem is even observed in mEC lesioned rats in which the substantially degraded CA1 activity on the return arms may have precluded that the trajectory is efficiently locally encoded. One possibility is that the CA3 network is a site for plasticity during the task phase when the trajectory is encoded and that information about the preceding trajectory is forwarded from CA3 to CA1 after the end of delay. This is in agreement with the finding that CA3 excitation of CA1 neurons is strongest on the stem in the alternation task (Fernandez-Ruiz et al., 2017) and that CA3 slow gamma promotes recall of upcoming trajectories (Zheng et al., 2016). Moreover, CA3 to CA1 synaptic efficiency has been reported to increase after mEC lesions (O'Reilly et al., 2014), which could at least partially account for the mild behavioral deficit in mEC lesioned rats and for the substantially more pronounced deficit with combined lesions.

Taken together, our results indicate that the entorhino-hippocampal circuit does not necessarily contribute with time-cell-based mechanisms or any other type of persistent activity to working memory over delay intervals. Our results point to an alternate mechanism by which mEC could affect working memory. One possibility is that the contribution of mEC to WM consists of supporting the distinct encoding of the past choice by plasticity mechanisms, which can later support the reemergence of distinct activity in the local network during retrieval. Alternatively, mEC could provide spatially distinct firing patterns that can induce persistent or sequential activity elsewhere in the brain, such as in prefrontal cortex. However, the latter possibility is less likely for longer retention intervals, when compensation by prefrontal areas for the loss of hippocampal inputs has been shown to diminish (Lee and Kesner, 2003). Accordingly, we show that at increasingly longer retention intervals, which make memory performance more definitely hippocampus and mEC dependent, there is diminishing evidence for the manifestation of hippocampal time cells, suggesting that other mechanisms than time cells and related types of sequential activity support WM.

STAR★METHODS

Detailed methods are provided in the online version of this paper and include the following:

- KEY RESOURCES TABLE
- CONTACT FOR REAGENT AND RESOURCE SHARING
- EXPERIMENTAL MODEL AND SUBJECT DETAILS
  - Subjects
- METHOD DETAILS
  - Surgical procedures
  - Behavior Apparatus
  - Behavioral Task
  - Neurohistological methods and tetrode locations
- QUANTIFICATION AND STATISTICAL ANALYSIS
  - Cell sorting and cell tracking
  - Cell classification
  - Rate maps
  - Spatial correlation
  - Correlation between time bins during the delay
  - Linear classifier
  - Spatial information
  - Rate differences on the stem and during the delay
  - Shuffling procedures
  - Statistical Analysis

SUPPLEMENTAL INFORMATION

Supplemental Information can be found online at https://doi.org/10.1016/j.neuron.2019.04.005.

ACKNOWLEDGMENTS

The authors would like to thank A. Dede for help with the perseveration analysis, as well as V. Alluri, S. Acosta, A. Schlenner, and C. Luong for assistance and technical support. This work was supported by the Walter Heiligenberg Professorship and NIH grants R01 NS086947, R01 MH100349, and T32 AG00216.

AUTHOR CONTRIBUTIONS

Conceptualization and Methodology, M.S., S.L., R.E.C., and J.K.L.; Software, S.L., D.T.Z., C.L., and S.A.; Formal Analysis, M.S. D.T.Z., C.L., and S.A.; Investigation, M.S., A.S., B.L.B., and N.G.; Writing – Original Draft, M.S. and S.L.; Writing – Review and Editing, M.S., S.L., J.K.L., and R.E.C.; Funding Acquisition, S.L., R.E.C., J.K.L., and M.S.; Supervision, S.L., J.K.L., and R.E.C.

DECLARATION OF INTERESTS

The authors declare no competing interests.

Received: October 3, 2018
Revised: February 5, 2019
Accepted: March 29, 2019
Published: May 2, 2019

SUPPORTING CITATIONS

The following references appear in the Supplemental Information: Newman and Hasselmo (2014) and Perez-Escobar et al. (2016).

REFERENCES

Aggleton, J.P., Hunt, P.R., and Rawlins, J.N. (1986). The effects of hippocampal lesions upon spatial and non-spatial tests of working memory. Behav. Brain Res. *19*, 133–146.

Ainge, J.A., van der Meer, M.A., Langston, R.F., and Wood, E.R. (2007). Exploring the role of context-dependent hippocampal activity in spatial alternation behavior. Hippocampus *17*, 988–1002.

Allen, T.A., Salz, D.M., McKenzie, S., and Fortin, N.J. (2016). Nonspatial Sequence Coding in CA1 Neurons. J. Neurosci. *36*, 1547–1563.

Baeg, E.H., Kim, Y.B., Huh, K., Mook-Jung, I., Kim, H.T., and Jung, M.W. (2003). Dynamics of population code for working memory in the prefrontal cortex. Neuron *40*, 177–188.

Barak, O., and Tsodyks, M. (2014). Working models of working memory. Curr. Opin. Neurobiol. *25*, 20–24.

Bower, M.R., Euston, D.R., and McNaughton, B.L. (2005). Sequential-context-dependent hippocampal activity is not necessary to learn sequences with repeated elements. J. Neurosci. *25*, 1313–1323.

Bragin, A., Jandó, G., Nádasdy, Z., Hetke, J., Wise, K., and Buzsáki, G. (1995). Gamma (40-100 Hz) oscillation in the hippocampus of the behaving rat. J. Neurosci. *15*, 47–60.

Buzsáki, G., and Moser, E.I. (2013). Memory, navigation and theta rhythm in the hippocampal-entorhinal system. Nat. Neurosci. *16*, 130–138.

Clark, R.E., Zola, S.M., and Squire, L.R. (2000). Impaired recognition memory in rats after damage to the hippocampus. J. Neurosci. *20*, 8853–8860.

Clark, R.E., Broadbent, N.J., Zola, S.M., and Squire, L.R. (2002). Anterograde amnesia and temporally graded retrograde amnesia for a nonspatial memory task after lesions of hippocampus and subiculum. J. Neurosci. *22*, 4663–4669.

Csicsvari, J., Hirase, H., Czurkó, A., Mamiya, A., and Buzsáki, G. (1999). Oscillatory coupling of hippocampal pyramidal cells and interneurons in the behaving Rat. J. Neurosci. *19*, 274–287.

de Lima, M.N., Luft, T., Roesler, R., and Schröder, N. (2006). Temporary inactivation reveals an essential role of the dorsal hippocampus in consolidation of object recognition memory. Neurosci. Lett. *405*, 142–146.

Diehl, G.W., Hon, O.J., Leutgeb, S., and Leutgeb, J.K. (2017). Grid and nongrid cells in medial entorhinal cortex represent spatial location and environmental features with complementary coding schemes. Neuron *94*, 83–92 e86.

Druckmann, S., and Chklovskii, D.B. (2012). Neuronal circuits underlying persistent representations despite time varying activity. Curr. Biol. *22*, 2095–2103.

Dudchenko, P.A., Wood, E.R., and Eichenbaum, H. (2000). Neurotoxic hippocampal lesions have no effect on odor span and little effect on odor recognition memory but produce significant impairments on spatial span, recognition, and alternation. J. Neurosci. *20*, 2964–2977.

Duva, C.A., Floresco, S.B., Wunderlich, G.R., Lao, T.L., Pinel, J.P., and Phillips, A.G. (1997). Disruption of spatial but not object-recognition memory by neurotoxic lesions of the dorsal hippocampus in rats. Behav. Neurosci. *111*, 1184–1196.

Eichenbaum, H. (2014). Time cells in the hippocampus: a new dimension for mapping memories. Nat. Rev. Neurosci. *15*, 732–744.

Ferbinteanu, J., and Shapiro, M.L. (2003). Prospective and retrospective memory coding in the hippocampus. Neuron *40*, 1227–1239.

Fernandez-Ruiz, A., Oliva, A., Nagy, G.A., Maurer, A.P., Berenyi, A., and Buzsaki, G. (2017). Entorhinal-CA3 dual-input control of spike timing in the hippocampus by theta-gamma coupling. Neuron *93*, 1213–1226 e1215.

Frank, L.M., Brown, E.N., and Wilson, M. (2000). Trajectory encoding in the hippocampus and entorhinal cortex. Neuron *27*, 169–178.

Fujisawa, S., Amarasingham, A., Harrison, M.T., and Buzsáki, G. (2008). Behavior-dependent short-term assembly dynamics in the medial prefrontal cortex. Nat. Neurosci. *11*, 823–833.

Fuster, J.M., and Alexander, G.E. (1971). Neuron activity related to short-term memory. Science *173*, 652–654.

Gill, P.R., Mizumori, S.J., and Smith, D.M. (2011). Hippocampal episode fields develop with learning. Hippocampus *21*, 1240–1249.

Girardeau, G., Benchenane, K., Wiener, S.I., Buzsáki, G., and Zugaro, M.B. (2009). Selective suppression of hippocampal ripples impairs spatial memory. Nat. Neurosci. *12*, 1222–1223.

Griffin, A.L., Eichenbaum, H., and Hasselmo, M.E. (2007). Spatial representations of hippocampal CA1 neurons are modulated by behavioral context in a hippocampus-dependent memory task. J. Neurosci. *27*, 2416–2423.

Hafting, T., Fyhn, M., Molden, S., Moser, M.B., and Moser, E.I. (2005). Microstructure of a spatial map in the entorhinal cortex. Nature *436*, 801–806.

Hales, J.B., Schlesiger, M.I., Leutgeb, J.K., Squire, L.R., Leutgeb, S., and Clark, R.E. (2014). Medial entorhinal cortex lesions only partially disrupt hippocampal place cells and hippocampus-dependent place memory. Cell Rep. *9*, 893–901.

Hales, J.B., Vincze, J.L., Reitz, N.T., Ocampo, A.C., Leutgeb, S., and Clark, R.E. (2018). Recent and remote retrograde memory deficit in rats with medial entorhinal cortex lesions. Neurobiol. Learn. Mem. *155*, 157–163.

Hammond, R.S., Tull, L.E., and Stackman, R.W. (2004). On the delay-dependent involvement of the hippocampus in object recognition memory. Neurobiol. Learn. Mem. *82*, 26–34.

Hargreaves, E.L., Rao, G., Lee, I., and Knierim, J.J. (2005). Major dissociation between medial and lateral entorhinal input to dorsal hippocampus. Science *308*, 1792–1794.

Henze, D.A., Borhegyi, Z., Csicsvari, J., Mamiya, A., Harris, K.D., and Buzsáki, G. (2000). Intracellular features predicted by extracellular recordings in the hippocampus in vivo. J. Neurophysiol. *84*, 390–400.

Heys, J.G., and Dombeck, D.A. (2018). Evidence for a subcircuit in medial entorhinal cortex representing elapsed time during immobility. Nat. Neurosci. *21*, 1574–1582.

Hölscher, C., Jacob, W., and Mallot, H.A. (2004). Learned association of allocentric and egocentric information in the hippocampus. Exp. Brain Res. *158*, 233–240.

Ito, H.T., Zhang, S.J., Witter, M.P., Moser, E.I., and Moser, M.B. (2015). A prefrontal-thalamo-hippocampal circuit for goal-directed spatial navigation. Nature *522*, 50–55.

Jadhav, S.P., Rothschild, G., Roumis, D.K., and Frank, L.M. (2016). Coordinated Excitation and Inhibition of Prefrontal Ensembles during Awake Hippocampal Sharp-Wave Ripple Events. Neuron *90*, 113–127.

Johnson, A., and Redish, A.D. (2007). Neural ensembles in CA3 transiently encode paths forward of the animal at a decision point. J. Neurosci. *27*, 12176–12189.

Kitamura, T., Macdonald, C.J., and Tonegawa, S. (2015). Entorhinal-hippocampal neuronal circuits bridge temporally discontiguous events. Learn. Mem. *22*, 438–443.

Koenig, J., Linder, A.N., Leutgeb, J.K., and Leutgeb, S. (2011). The spatial periodicity of grid cells is not sustained during reduced theta oscillations. Science *332*, 592–595.

Kraus, B.J., Brandon, M.P., Robinson, R.J., 2nd, Connerney, M.A., Hasselmo, M.E., and Eichenbaum, H. (2015). During running in place, grid cells integrate elapsed time and distance run. Neuron *88*, 578–589.

Lee, I., and Kesner, R.P. (2003). Time-dependent relationship between the dorsal hippocampus and the prefrontal cortex in spatial memory. J. Neurosci. *23*, 1517–1523.

Lee, I., Griffin, A.L., Zilli, E.A., Eichenbaum, H., and Hasselmo, M.E. (2006). Gradual translocation of spatial correlates of neuronal firing in the hippocampus toward prospective reward locations. Neuron *51*, 639–650.

Liu, D., Gu, X., Zhu, J., Zhang, X., Han, Z., Yan, W., Cheng, Q., Hao, J., Fan, H., Hou, R., et al. (2014). Medial prefrontal activity during delay period contributes to learning of a working memory task. Science *346*, 458–463.

MacDonald, C.J., Lepage, K.Q., Eden, U.T., and Eichenbaum, H. (2011). Hippocampal "time cells" bridge the gap in memory for discontiguous events. Neuron *71*, 737–749.

Mankin, E.A., Sparks, F.T., Slayyeh, B., Sutherland, R.J., Leutgeb, S., and Leutgeb, J.K. (2012). Neuronal code for extended time in the hippocampus. Proc. Natl. Acad. Sci. USA *109*, 19462–19467.

McKenzie, S., Frank, A.J., Kinsky, N.R., Porter, B., Rivière, P.D., and Eichenbaum, H. (2014). Hippocampal representation of related and opposing memories develop within distinct, hierarchically organized neural schemas. Neuron *83*, 202–215.

Miao, C., Cao, Q., Ito, H.T., Yamahachi, H., Witter, M.P., Moser, M.B., and Moser, E.I. (2015). Hippocampal remapping after partial inactivation of the medial entorhinal cortex. Neuron *88*, 590–603.

Miller, V.M., and Best, P.J. (1980). Spatial correlates of hippocampal unit activity are altered by lesions of the fornix and endorhinal cortex. Brain Res. *194*, 311–323.

Mongillo, G., Barak, O., and Tsodyks, M. (2008). Synaptic theory of working memory. Science *319*, 1543–1546.

Mumby, D.G., Wood, E.R., Duva, C.A., Kornecook, T.J., Pinel, J.P., and Phillips, A.G. (1996). Ischemia-induced object-recognition deficits in rats are attenuated by hippocampal ablation before or soon after ischemia. Behav. Neurosci. *110*, 266–281.

Newman, E.L., and Hasselmo, M.E. (2014). CA3 sees the big picture while dentate gyrus splits hairs. Neuron *81*, 226–228.

O'Reilly, K.C., Alarcon, J.M., and Ferbinteanu, J. (2014). Relative contributions of CA3 and medial entorhinal cortex to memory in rats. Front. Behav. Neurosci. *8*, 292.

Olton, D.S., Becker, J.T., and Handelmann, G.E. (1979). Hippocampus, space, and memory. Behav. Brain Sci. *2*, 313–322.

Pastalkova, E., Itskov, V., Amarasingham, A., and Buzsáki, G. (2008). Internally generated cell assembly sequences in the rat hippocampus. Science *321*, 1322–1327.

Perez-Escobar, J.A., Kornienko, O., Latuske, P., Kohler, L., and Allen, K. (2016). Visual Landmarks Sharpen Grid Cell Metric and Confer Context Specificity to Neurons of the Medial Entorhinal Cortex. Elife *23*, https://doi.org/10.7554/eLife.16937.

Pfeiffer, B.E., and Foster, D.J. (2013). Hippocampal place-cell sequences depict future paths to remembered goals. Nature *497*, 74–79.

Prusky, G.T., Douglas, R.M., Nelson, L., Shabanpoor, A., and Sutherland, R.J. (2004). Visual memory task for rats reveals an essential role for hippocampus and perirhinal cortex. Proc. Natl. Acad. Sci. USA *101*, 5064–5068.

Rampon, C., Tang, Y.P., Goodhouse, J., Shimizu, E., Kyin, M., and Tsien, J.Z. (2000). Enrichment induces structural changes and recovery from nonspatial memory deficits in CA1 NMDAR1-knockout mice. Nat. Neurosci. *3*, 238–244.

Robinson, N.T.M., Priestley, J.B., Rueckemann, J.W., Garcia, A.D., Smeglin, V.A., Marino, F.A., and Eichenbaum, H. (2017). Medial entorhinal cortex selectively supports temporal coding by hippocampal neurons. Neuron *94*, 677–688 e676.

Rueckemann, J.W., DiMauro, A.J., Rangel, L.M., Han, X., Boyden, E.S., and Eichenbaum, H. (2016). Transient optogenetic inactivation of the medial entorhinal cortex biases the active population of hippocampal neurons. Hippocampus *26*, 246–260.

Salz, D.M., Tiganj, Z., Khasnabish, S., Kohley, A., Sheehan, D., Howard, M.W., and Eichenbaum, H. (2016). Time cells in hippocampal area CA3. J. Neurosci. *36*, 7476–7484.

Sasaki, T., Piatti, V.C., Hwaun, E., Ahmadi, S., Lisman, J.E., Leutgeb, S., and Leutgeb, J.K. (2018). Dentate network activity is necessary for spatial working memory by supporting CA3 sharp-wave ripple generation and prospective firing of CA3 neurons. Nat. Neurosci. *21*, 258–269.

Schlesiger, M.I., Cannova, C.C., Boublil, B.L., Hales, J.B., Mankin, E.A., Brandon, M.P., Leutgeb, J.K., Leibold, C., and Leutgeb, S. (2015). The medial entorhinal cortex is necessary for temporal organization of hippocampal neuronal activity. Nat. Neurosci. *18*, 1123–1132.

Schlesiger, M.I., Boublil, B.L., Hales, J.B., Leutgeb, J.K., and Leutgeb, S. (2018). Hippocampal global remapping can occur without input from the medial entorhinal cortex. Cell Rep. *22*, 3152–3159.

Shapiro, M.L., and Eichenbaum, H. (1999). Hippocampus as a memory map: synaptic plasticity and memory encoding by hippocampal neurons. Hippocampus *9*, 365–384.

Singer, A.C., Karlsson, M.P., Nathe, A.R., Carr, M.F., and Frank, L.M. (2010). Experience-dependent development of coordinated hippocampal spatial activity representing the similarity of related locations. J. Neurosci. *30*, 11586–11604.

Skaggs, W.E., McNaughton, B.L., Wilson, M.A., and Barnes, C.A. (1996). Theta phase precession in hippocampal neuronal populations and the compression of temporal sequences. Hippocampus *6*, 149–172.

Smith, D.M., and Mizumori, S.J. (2006). Learning-related development of context-specific neuronal responses to places and events: the hippocampal role in context processing. J. Neurosci. *26*, 3154–3163.

Stokes, M.G. (2015). 'Activity-silent' working memory in prefrontal cortex: a dynamic coding framework. Trends Cogn. Sci. *19*, 394–405.

Suh, J., Rivest, A.J., Nakashiba, T., Tominaga, T., and Tonegawa, S. (2011). Entorhinal cortex layer III input to the hippocampus is crucial for temporal association memory. Science *334*, 1415–1420.

Takehara, K., Kawahara, S., and Kirino, Y. (2003). Time-dependent reorganization of the brain components underlying memory retention in trace eyeblink conditioning. J. Neurosci. *23*, 9897–9905.

Tiganj, Z., Jung, M.W., Kim, J., and Howard, M.W. (2017). Sequential firing codes for time in rodent medial prefrontal cortex. Cereb. Cortex *27*, 5663–5671.

Wood, E.R., Dudchenko, P.A., Robitsek, R.J., and Eichenbaum, H. (2000). Hippocampal neurons encode information about different types of memory episodes occurring in the same location. Neuron *27*, 623–633.

Yang, S.T., Shi, Y., Wang, Q., Peng, J.Y., and Li, B.M. (2014). Neuronal representation of working memory in the medial prefrontal cortex of rats. Mol. Brain *7*, 61.

Zheng, C., Bieri, K.W., Hsiao, Y.T., and Colgin, L.L. (2016). Spatial sequence coding differs during slow and fast gamma rhythms in the hippocampus. Neuron *89*, 398–408.

STAR★METHODS

KEY RESOURCES TABLE

REAGENT or RESOURCE	SOURCE	IDENTIFIER
Chemicals, Peptides, and Recombinant Proteins		
Isoflurane	MWI	Cat #: NDC 13985-528-60
Buprenorphine	MWI	Cat #: 29308
Plantinic acid for platinum plating	Sigma-Aldrich	Cat #: 206083; CAS 18497-13-7
Sodium pentobarbital	MWI	Cat #: 15199
Formaldehyde	EMD	Cat #: FX-0415-4; CAS 50-00-0
NMDA	Tocris Bioscience	Cat #: 0114; CAS 6384-92-5
Ibotenic acid	Tocris Bioscience	Cat #: 0285; CAS 2552-55-8
Cresyl violet	EMD	Cat #: M-19012; CAS 10510-54-0
Software and Algorithms		
MClust	A.D. Redish	http://redishlab.neuroscience.umn.edu/MClust/MClust.html
MATLAB v 2015b	Mathworks	RRID: SCR_001622
Other		
Hyperdrive	Custom built; Designed by B McNaughton	US Patent: US5928143 A
Platinum-Iridium tetrode wire	California fine wire company	Cat #: CFW0011873
Freezing microtome	Leica	Model: SM 2000R
Digital Neuralynx recording system	Neuralynx	Model: Digital Lynx SX

CONTACT FOR REAGENT AND RESOURCE SHARING

Further information and requests for resources and datasets should be directed to and will be fulfilled by the Lead Contact, Stefan Leutgeb (sleutgeb@ucsd.edu).

EXPERIMENTAL MODEL AND SUBJECT DETAILS

Subjects

All animal experiments were approved by the University of California, San Diego Institutional Animal Care and Use Committee and conducted according to National Institutes of Health guidelines. The subjects were 20 experimentally naive, male Long–Evans rats weighing between 300 g and 350 g. Rats were housed individually on a reversed 12 h light/dark cycle. Behavioral testing and recording sessions were performed in the dark phase of the light-dark cycle. During periods of behavioral testing and recording, rats were food restricted and maintained at ~85% of their *ad libitum* weight. The rats were divided into three groups, a group with nearly complete NMDA lesions of the medial entorhinal cortex (mEC; n = 10), a group with combined lesions of the mEC and the hippocampus (mEC+H; n = 5), and a control group (Control; n = 9). The animals were randomly assigned to one of the groups.

METHOD DETAILS

Surgical procedures

All surgeries were performed using aseptic procedures. Anesthesia was maintained throughout surgery with isoflurane gas (0.8%–2.0% isoflurane delivered in O_2 at 1 L/min), and buprenorphine (0.02 mg/kg) was administered as an analgesic. Animals were positioned in a Kopf stereotaxic instrument, and the incisor bar was adjusted until bregma was level with lambda. The bone overlying the target site was removed using a high-speed drill. The control group underwent these initial surgical procedures, but injections into the brain were not performed. The two experimental groups received excitotoxic lesions of either mEC or of mEC and hippocampus combined. For mEC lesions, NMDA was used as an excitatory analog of glutamic acid. NMDA (Tocris) was dissolved in aCSF (Harvard Instruments) to provide a solution with a concentration of 10 mg/mL and was injected at a rate of 0.1 μl/min using a 10 μl Hamilton (Reno, NV) syringe mounted on a stereotaxic frame and held with a Kopf model 5000 microinjector. The antero-posterior (AP) coordinate was measured from the anterior border of the transverse sinus, and the needle was inserted at medio-lateral

(ML) ± 4.6 mm with an angle of 22° moving from posterior to anterior. The syringe needle was lowered 5.2 mm from the dura and left in place for 1 min before the start of the injection. NMDA was injected into 8 sites [-5.2, −4.7, −4.2, −3.7, −3.2, −2.7, −2.2, and −1.7 mm dorsoventral (DV) from dura, 0.87 μl of toxin at each injection site], and was intended to damage the complete area of medial entorhinal cortex. The syringe needle was left in place for 1 min after the injection to reduce the spread of drug up the needle tract. For the additional hippocampal lesions in the combined lesion group, corresponding procedures were used with the following modifications. Instead of NMDA, ibotenic acid (Tocris) was dissolved in 1X PBS to provide a solution with a concentration of 10 mg/mL, pH 7.4. The toxin was injected into 18 sites (all coordinates are in mm, AP is relative to bregma, ML is relative to lambda, DV relative to dura, volume is in μl; AP −2.4, ML ± 1.0, DV −3.5, 0.025 μl; AP −3.2, ML ± 1.4, DV −3.1, −2.3, 0.05 μl; AP −3.2, ML ± 3.0, DV −2.7, 0.04; AP −4.0, ML ± 2.5, DV −2.8, −1.8, 0.05 μl; AP −4.0, ML ± 3.7, DV −2.7,0.04 μl; AP −4.8, ML ± 4.9, DV −7.2, −6.4, 0.05 μl; AP −4.8, ML ± 4.3, DV −7.7, −7.1, −3.5, 0.085 μl; AP −5.4, ML ± 4.2, DV −4.4, −3.9, 0.05 μl; AP −5.4, ML ± 5.0, DV −6.6, −5.9, −5.2, −4.5, 0.12 μl) on each side of the brain and was intended to damage the dorsal and ventral hippocampus. After completion of the injections, the skin was sutured, and the animal was allowed to recover from anesthesia on a water-circulating heating pad. All animals received postoperative care for at least 5 days after surgery.

After an interval of at least 9 weeks to allow for recovery and initial behavioral testing, all animals of the mEC lesion and control groups underwent a second surgery to implant a fourteen-tetrode recording assembly. The second surgery used the same general procedures as the first surgery but tetrodes were implanted in the cortical area above the dorsal hippocampus instead of performing injections. The recording assembly consisted of 14 tetrodes that were each constructed by twisting four 17 μm polyimide coated platinum-iridium (90%/10%) wires. The electrode tips were plated with platinum to reduce the impedances to 200–300 kΩ at 1 kHz. The tetrodes were arranged into a bundle targeted to the hippocampus in the right hemisphere (AP: 4.0 mm, ML: ± 2.8 mm).

Behavior Apparatus

Behavior was conducted in a T-maze that was modified to include return arms and thus had a figure-8 shape (Figure S3A). The maze was constructed from a series of interlocking gray hard plastic runways that were 10 cm wide and fitted with 2 cm tall ridges of the same material on each side. The center runway that forms the stem of the figure-8 maze was 150 cm long and 10 cm wide, as were the right and left return arms. A 101 cm long crosspiece connected the center arm to the right and left return arms at the top and at the bottom of the maze. One automatic and one manual barrier were used to interpose a delay interval between some of the trials. The delay zone was at the base of the center arm and 25 cm long. Food-rewards (chocolate sprinkles) were delivered at the distal ends of each of the top arms after the animals made a correct choice. The figure-8 maze was elevated 50 cm above the floor and positioned within an open environment with prominent and constant visual cues. A light source in a corner of the room (approximately 1 m from the maze and 2 m from the sleep chamber) kept the environment dimly illuminated.

Behavioral Task

Before the beginning of the behavioral training, rats were given 4 weeks to recover from the lesion surgery. At the start of the training, rats were handled, were given chocolate sprinkles in their home cages for three days, and were familiarized with the room where the testing would take place by allowing them to freely explore the maze for 10 min with chocolate sprinkles scattered over the maze (“habituation day”). The next day, the first stage of testing began by placing the rat at the base of the center arm of the figure-8 maze. During this stage, a barrier was used to force the rat to enter one of the two side arms where a reward was delivered. After consuming the reward, the rat was guided to return to the base of the center arm and was allowed to run to the opposite connecting arm in a figure-8 pattern. The rat was prevented from retracing its route at any point. Each session was 20 min long or 30 trials, whichever came first. This procedure was repeated, using barriers on alternating arms until the animals ran the pattern consistently during two consecutive days. In the second stage, the use of a barrier at the choice point was phased out and the rats were able to enter either arm each time they reached the end of the stem. However, they were rewarded only for running alternating arm entries in a figure-8 pattern, and they were prevented from retracing their steps at any point. Second stage sessions were 20 min long or 30 trials, whichever came first. Rats were trained to a criterion performance of at least 90% correct trials on two of three consecutive days. The third stage started once the rats reached this criterion and included trials with delay. In each daily session, rats received 30 trials grouped into three blocks of 10 trials (no delay, 10-s delay and 60-s delay for 7 mEC lesioned and 8 control rats, only these rats were used for behavioral analysis; no delay, 2-s delay, and 10-s delay for 3 mEC lesioned and 1 control rat, only the no delay and 10-s delay of these rats was used for analysis of hippocampal recordings). The order of the three blocks was pseudorandomized every day. During delay trials, as the rat returned to the base of the stem after the last trial of the previous block, two barriers were placed to confine the rat to a 25 cm zone at the base of the stem. At the end of the delay interval, the barrier that blocked access to the center arm was lowered and the rat was free to traverse the stem and make its next choice. After the rat made a choice and ate the reward, it returned to the delay zone on the center arm. This stage continued for 14 days.

Animals were then fed *ad libitum* for at least a week before the second surgery during which the recording assembly was implanted. During the recovery period from the second surgery, tetrodes were slowly advanced into the CA1 and CA3 areas of the hippocampus. After five days of recovery, rats started to run some trials without delays in order to get habituated to the recording cable that now connected the electrode assembly to the recording system. During tetrode advancement and recordings, the signals were preamplified with a unity gain headstage and were recorded with a data acquisition system with 64 digitally programmable differential amplifiers (Neuralynx, Tucson, AZ, USA). Spike waveforms above a threshold of 40-45 μV were time-stamped and digitized at 32 kHz for

1 ms. The rat's position was tracked at 30 Hz by recording the position of light-emitting diodes that were placed above the head. Local field potentials were acquired by recording one channel of each tetrode with the filters set to the 1-450 Hz band. As expected (Bragin et al., 1995) sharp wave ripples were not diminished by the mEC lesion and could therefore be used to guide electrode advancement into the cell layers in all rats. Recording in the figure-8 maze began when tetrodes were stably positioned in the CA1 and/or CA3 cell layer. Spikes and local field potentials were recorded during the alternation task and also while the rat was resting in a transparent holding chamber located in the same room for 1 hour at the beginning (sleep 1) and 1 hour at the end of each recording day (sleep2). Each animal ran one session per day for 6 to 12 days. Data collection and analysis were not performed blind to the conditions of the experiment.

Neurohistological methods and tetrode locations

At the end of the recording procedures, rats were administered an overdose of sodium pentobarbital and perfused transcardially with a phosphate buffered solution followed by 4% paraformaldehyde solution (in 0.1 M phosphate buffer). Brains were then removed from the skull and kept in a solution of 4% paraformaldehyde for 24 h before they were transferred to a 30% sucrose solution where they remained for an average of 48 hours. Sagittal sections (40 μm) were cut with a freezing microtome beginning just lateral to the hippocampus and continuing medially through the hippocampus and mEC of each hemisphere. Every section was mounted and stained with cresyl violet to identify the hippocampal tetrode locations. Every fourth section was used to quantify the lesion extent with the Cavalieri method, as previously described (Hales et al., 2014). For MEC lesions, the volume of the spared tissue in the mEC layer II, mEC layer III, mEC deep layers, dorsal parasubiculum, and ventral parasubiculum was quantified. In the mEC-lesioned rats, cells in the superficial layers were either completely absent or, when small patches of cells were discernable, showed signs of disorganization and necrosis such as multipolar processes and fragmented nuclei (Schlesiger et al., 2018). Damage to brain areas other than the lesion targets and parasubiculum were not substantial, as previously reported (Hales et al., 2014). The percent of damage was calculated by normalizing the volume of spared tissue to the volume of controls with the formula below.

$$\%\ of\ damage = \left(1 - \frac{spared\ \ estimated\ \ volume}{average\ \ volume\ \ in\ \ control\ \ group}\right) \cdot 100$$

Tetrode trajectories through hippocampus were determined from 3D reconstruction of the sectioned tissue. Based on records of the systematic movement of tetrodes through the brain and the trajectory information, complemented by records of LFP profiles, tetrode locations on each recording day were assigned to either CA1 or CA3 regions.

QUANTIFICATION AND STATISTICAL ANALYSIS

Cell sorting and cell tracking

Single units were manually sorted using MClust (version 3.5, written by A. David Redish; http://redishlab.neuroscience.umn.edu/MClust/MClust.html) and customized by Mankin et al. (2012). Clusters that persisted in the same region of parameter space throughout a whole session were accepted for analysis when the action potential amplitude/shape of spikes in each cluster were distinct from noise signals and remained inside the same set of cluster boundaries throughout the session. Recordings during rest periods (before and after the task) were used to confirm recording stability during the experiment and to identify hippocampal cells that were silent or fired at low rates during behavior. Up to three recording sessions per rat were considered for analysis and, while we tried to avoid double-counting cells by advancing tetrodes and/or by analyzing non-consecutive days, in some cases the same cells could have been recorded in more than one analysis day.

Cell classification

Neurons were classified as putative interneurons versus putative principal neurons using a criterion applied to the relationship between spike ratio and spike rate (Csicsvari et al., 1999). Briefly, extracellular recordings of action potentials (spikes) were inverted resulting in an early upward peak (peak1) and a later downward peak (peak2). Mean spike ratios were calculated by dividing the absolute amplitude of peak 1 by the absolute amplitude of peak 2. The amplitude of the first peak is related to the rise time of the depolarization, and the amplitude of the second peak is related to the decay time of repolarization (Henze et al., 2000). Spike ratios are thus approximately equal to 1 for cells that have comparable rates of depolarization and repolarization, and interneurons rather than principal cells are known to have repolarization rates that are approximately equal to depolarization rates. Therefore, cells that had spike rates below 15 Hz and spike ratios above 1 were considered putative principal cells and cells that had spike rates above 15 Hz and spike ratios below 1 were considered putative interneurons. Interneurons were excluded from the analysis.

Rate maps

For the illustration of rate maps in Figure 2A, the figure-8 maze was divided into 5 cm x 5 cm bins. Spatial firing rate distributions were constructed by summing the total number of spikes that occurred in each location bin, dividing by the amount of time that the animal spent in that location, and then smoothing with a boxcar filter (Koenig et al., 2011). For quantitative analysis, the animal's path along the figure-8 maze was linearized, left-turn and right-turn paths were separated with each lap beginning and ending at the reward locations. Spikes rates were then calculated for each 5 cm-long segment along the maze tracks and smoothed with a one dimensional

version of the boxcar filter. The linearized rate maps were used to determine peak rates, the spatial information, and rate differences between left and right trajectories. Only correct trials were analyzed.

Spatial correlation

The consistency of each cell's spatial firing pattern was measured by calculating, for each pair of left-turn trials and for each pair of right-turn trials, the Pearson's correlation between path segments at corresponding locations. Only correct trials were analyzed, and maze segments at the delay site were excluded. Pairwise comparisons in which the rates in all maze segments were less than 2 Hz were excluded. For each cell, the average correlation coefficient over all pairs of left-turn trials and the average over all pairs of right-turn trials was calculated, and the maximum of the two values was selected. The maximum was used so that cells with a place field on only one side of the maze would be assigned the correlation value from the trial type with the field. In addition to calculating spatial correlation coefficients between trials, we also averaged the firing rates over all left-turn trials and over all right-turn trials. These averages were used to calculate the spatial correlation between corresponding segments on the right and left side of the figure-8 maze. Maze segments on the stem were excluded when calculating the correlation between the two sides.

Correlation between time bins during the delay

In order to evaluate whether cells fired in a sequential manner during the delay, we computed Pearson's correlations between the firing rates in time bins over the delay interval. Each bin was 500 ms long and was smoothed by averaging over a 2500 ms window that was centered on the bin. Animals ran two blocks of 10 s delay trials and two blocks of 60 s delay trials in a daily session. Firing rate bins over the delay period in correct left-turn trials from the first block of 10 s delay trials were compared to firing rate bins in correct left-turn trials from the second block of 10 s delay trials. Similarly, firing rate bins in correct right-turn trials from the first block were compared to firing rate bins in correct right-turn trials from the second block. In addition, we also compared firing rate bins throughout the delay in correct left-turn trials with firing rate bins in correct right-turn trials of the same block. The same calculations were performed for blocks of trials with the 60 s delay. Cells had to exceed a peak firing rate of 2 Hz in at least one time bin to be considered active during the delay and to be included in the analysis. In addition, we computed correlations using time bins after splitting the delay lengths (10 s and 60 s) into 5 s intervals. Finally, we examined whether time cells are coding for relative or absolute timing (MacDonald et al., 2011) across the two different delay conditions. To test for absolute timing, we performed a correlation between each time bin in the 10 s delay and the time bins over the first 10 s of the 60 s delay. To test for relative timing, we compressed the data over the 60 s delay into the same number of bins as in the 10 s delay condition and performed correlations between the two sets of time bins.

Linear classifier

To evaluate whether the population activity during the delay contained any information about trial type, we constructed population vectors in time intervals of 1 s length and z-scored them cell-wise using mean and standard deviation over time bins. Z-scored population vectors were then randomly divided into a training and a test set for a linear classifier (MATLAB's svm_train) to distinguish left and right turns within each 10 s interval of the 60 s delay period. We also trained 100 classifiers on the same data with randomly shuffled turn labels (left or right). We compared the left-right prediction from the classifier (correct classification rate, CCR) between real and shuffled data in two ways. First, we took the proportion of sessions in which the CCR from the real data was in the upper 95% quantile of the shuffled data. Second, we computed the z score of the CCR with respect to the shuffle distribution of CCRs. Moreover, we performed the classification in two ways, one in which we assigned left/right labels from the future turn direction and one in which we assigned the labels from the past turn direction. For only the analysis using the linear classifier, but not for other analyses in the manuscript, we included correct and incorrect trials because there was otherwise not a sufficient number of trials in the mEC lesioned animals to perform the analysis.

Spatial information

The information score describes the information density per spike and was calculated as described by (Skaggs et al., 1996),

$$I = \sum_{i=1}^{N} p_i \frac{\lambda_i}{\lambda} log_2 \frac{\lambda_i}{\lambda}$$

where I is the information density measured in bits per spike, i is the index of the pixels of the place field, p_i is the probability of the rat being at location i, λ_i is the average firing rate of the cell when the rat is at location i, and λ is the total average firing rate.

Rate differences on the stem and during the delay

Rate differences between correct trials with an upcoming left-turn or an upcoming right-turn were calculated by subtracting the average firing rate of each cell in left-turn trials from the rate in right-turn trials and by dividing the difference by the sum of the rates for both trial types. A two-fold rate difference (score: 0.33) was taken as the minimum criterion to consider a cell's firing distinct between trial types. Only correct trials were analyzed.

Shuffling procedures

To generate distributions that are shuffled in space, we shifted the spatial firing patterns on the two sides of the maze with respect to each other by random distances that were at least 10 spatial bins apart. This shuffling procedure retains the spatial distributions of activity patterns but not the correspondence between matching positions. Using the shuffled data, we calculated both the trial by trial spatial correlations between the same trial type and the left versus right spatial correlations as above. For rate differences, shuffling by trial-type was preformed to determine whether rate differences on the stem and during the delays were trial-type dependent.

Statistical Analysis

Two-way ANOVAs were used to analyze behavioral data (Group x Delay) and sequence firing (Trial type x Block). Tukey's and Sidak multiple comparisons tests were used to analyze interactions. Linear regressions were used to analyze improvement in WM performance and to determine the extent to which the degree of mEC and parasubiculum damage was related to behavioral performance. Kolmogorov-Smirnov (KS) tests were performed to analyze differences between distributions, Mann-Whitney tests for between-group comparisons, and Wilcoxon tests for one-sample comparisons. Chi-square tests were used to test whether observed fractions of active cells differed from the expected fractions.

Neuron, Volume *102*

Supplemental Information

Time Cells in the Hippocampus Are Neither Dependent on Medial Entorhinal Cortex Inputs nor Necessary for Spatial Working Memory

Marta Sabariego, Antonia Schönwald, Brittney L. Boublil, David T. Zimmerman, Siavash Ahmadi, Nailea Gonzalez, Christian Leibold, Robert E. Clark, Jill K. Leutgeb, and Stefan Leutgeb

FIGURE S1

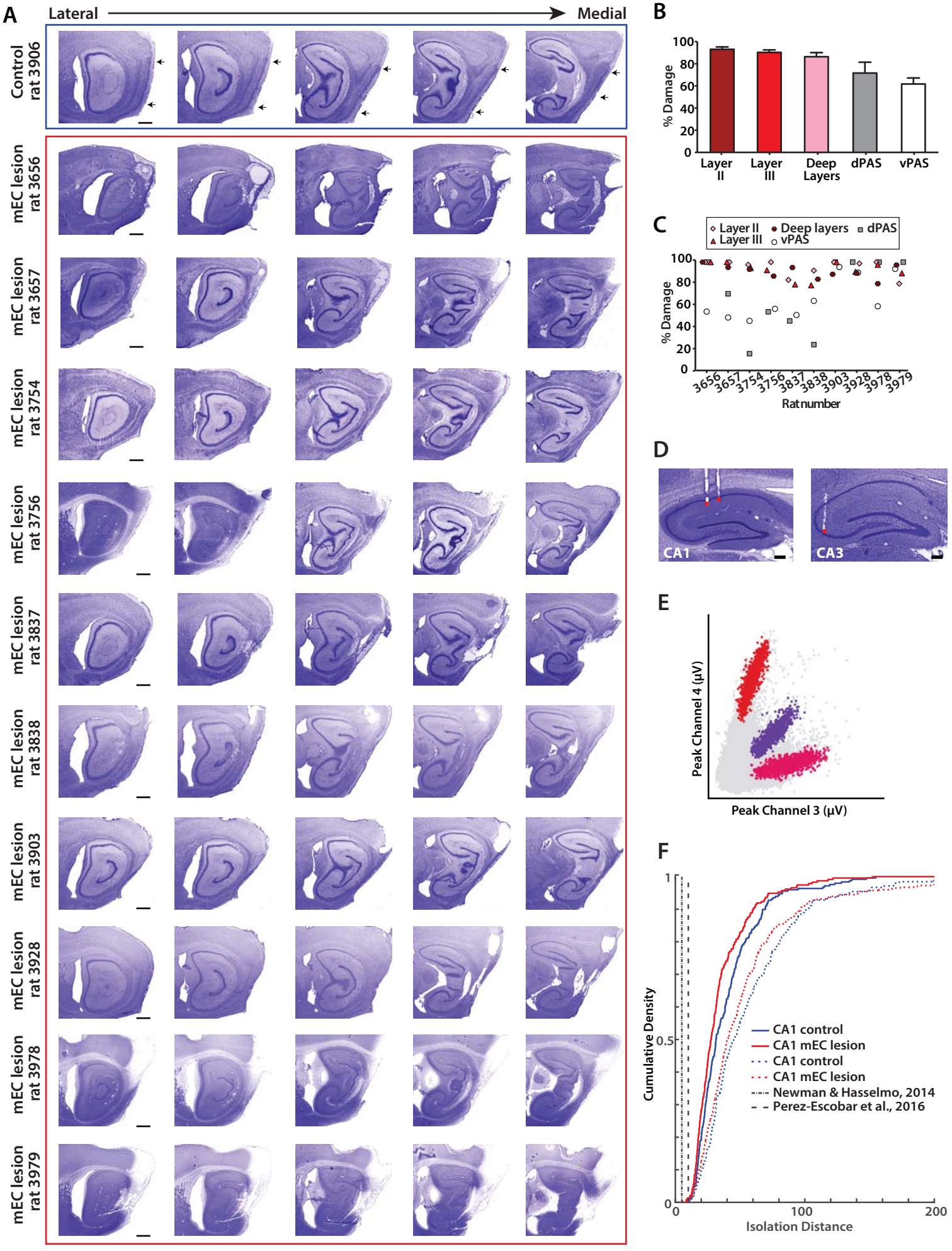
A
Lateral
Medial
Control rat 3906
mEC lesion rat 3656
mEC lesion rat 3657
mEC lesion rat 3754
mEC lesion rat 3756
mEC lesion rat 3837
mEC lesion rat 3838
mEC lesion rat 3903
mEC lesion rat 3928
mEC lesion rat 3978
mEC lesion rat 3979
B
% Damage
Layer II
Layer III
Deep Layers
dPAS
vPAS
C
Layer II
Layer III
Deep layers
vPAS
dPAS
% Damage
3656
3657
3754
3756
3837
3838
3903
3928
3978
3979
Rat number
D
CA1
CA3
E
Peak Channel 4 (μV)
Peak Channel 3 (μV)
F
Cumulative Density
CA1 control
CA1 mEC lesion
CA1 control
CA1 mEC lesion
Newman & Hasselmo, 2014
Perez-Escobar et al., 2016
Isolation Distance

Figure S1. MEC lesions were nearly complete in all mEC-lesioned subjects, and recording quality was not reduced by the lesion extent. Related to Figure 1 and 2.

(A) Detailed illustration of complete series of sagittal sections. Scale bar = 500 μm. Top: representative series of sagittal sections from a control rat. Arrows indicate the dorsal and ventral borders of mEC. The ten rows below are the series from all the mEC-lesioned rats in the study. (B) Average lesion size (n = 10 rats) of mEC layer II, layer III, deep layers (V/VI), dorsal parasubiculum (dPAS), and ventral parasubiculum (vPAS). Error bars represent SEM. (C) Percentage of lesioned tissue for each of the mEC-lesioned rats. (D) Example CA1 (top) and CA3 (bottom) tetrode tracks. Red dots indicate the end of the tracks in the pyramidal cell layer. Scale bars = 250 μm. (E) Example of cluster quality in an mEC-lesioned rat. (F) Cluster isolation distance was calculated for all recorded CA1 and CA3 cells in mEC-lesioned and control rats. Although there was a significant difference between mEC-lesioned and control CA1 cells ($p = 0.007$, KS test, n = 240 and 248 cells in the mEC lesion and control groups respectively), over 99% of our clusters had an isolation distance that was greater than previously published cutoffs [dashed gray lines: isolation distance of 5 (Newman and Hasselmo, 2014) and 10 (Perez-Escobar et al., 2016)]. No significant differences in cluster quality were found between groups in CA3 (n = 392 and 233 cells in the mEC lesion and control groups, respectively).

FIGURE S2

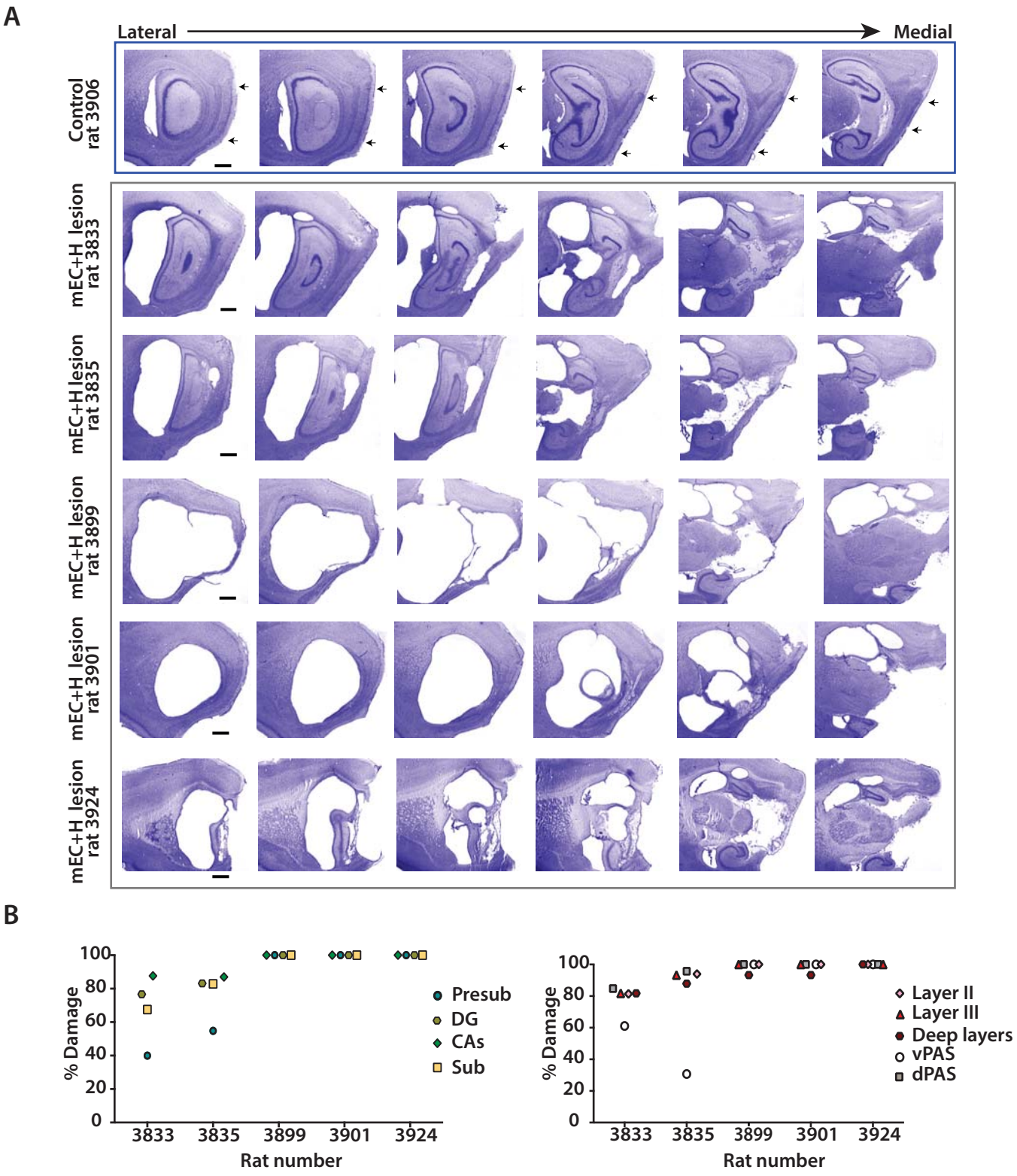

Figure S2. Combined lesions of the mEC and the hippocampus were nearly complete. Related to Figure 1.
(A) Series of sagittal sections from a representative control rat (top) and from the five combined mEC+H lesion rats in the study. Scale bar = 500 μm. (B) Percent lesioned tissue for each of the mEC+H lesioned rats (n = 5). Left and right panels quantify hippocampal and entorhinal damage, respectively. Subiculum (SUB), CA layers (CAs), dentate gyrus (DG), presubiculum (PRESUB), mEC layer II, layer III, deep layers (V/VI), dorsal parasubiculum (dPAS), and ventral parasubiculum (vPAS) are shown separately.

FIGURE S3

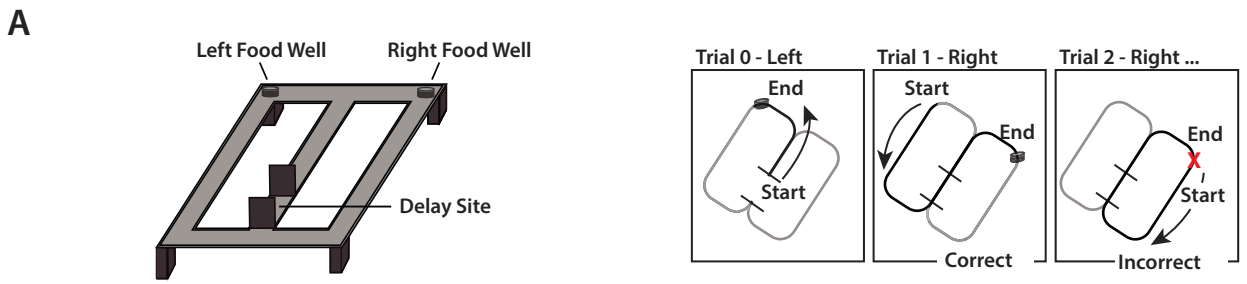
A
Left Food Well
Right Food Well
Delay Site
Trial 0 - Left
Trial 1 - Right
Trial 2 - Right ...
End
Start
End
Start
End
Start
Correct
Incorrect
B
No delay
10 s delay
60 s delay
% Correct choices
Days
control
mEC lesion
mEC+H lesion
C mEC lesion group
% mEC lesion volume
D
% Parasubiculum lesion volume
E mEC + H lesion group
**
F

Figure S3. WM performance improved throughout training, except in the combined lesion group, and there was generally no relation between lesion volume and WM performance. Related to Figure 1 and Table S3.
(A) Schematic of the figure-8 maze and of trials in the spatial alternation task. During training before tetrode implantation (Day 1-12), rats performed 10 trials (one block) of each condition (no delay, 10-s and 60-s delay). During recording sessions (Day 12-18) all rats performed two blocks of each condition in a pseudorandom order. (B) Percent correct choices on each day with stippled lines indicating chance level. Linear regression analyses were performed per group and per delay condition. (Left) No delay trials. Control (n = 8) and combined mEC+H lesioned rats (n = 5) showed a minor performance improvement over days ($r^2 = 0.1$, $p < 0.0001$ and $r^2 = 0.09$, $p = 0.0043$, respectively). (Middle) 10 s delay trials. Control and mEC-lesioned (n = 7) rats improved their WM performance with training ($r^2 = 0.23$ and $r^2 = 0.11$, respectively, $p < 0.0001$). (Right) 60 s delay trials. Control and mEC-lesioned rats improved their WM with training ($r^2 = 0.03$, $p = 0.0141$ and $r^2 = 0.11$, $p < 0.0001$, respectively). (C) Linear regression analyses comparing percent correct choices with mEC lesion volume for each delay condition. Stippled lines indicate chance level performance. WM performance during the recording phase did not depend on the mEC lesion volume. (D) Same as C, but for parasubiculum. WM performance during the recording phase did not depend on the lesion volume in parasubiculum. (E) Linear regression analyses comparing percent correct choices with mEC lesion volume in the combined lesion group. WM performance during the recording phase in the 10 s delay condition was worse in animals with larger mEC lesions. ** $p < 0.01$ (F) Same as E, but for parasubiculum. WM performance during the recording phase did not depend on lesion volume in the parasubiculum.

FIGURE S4

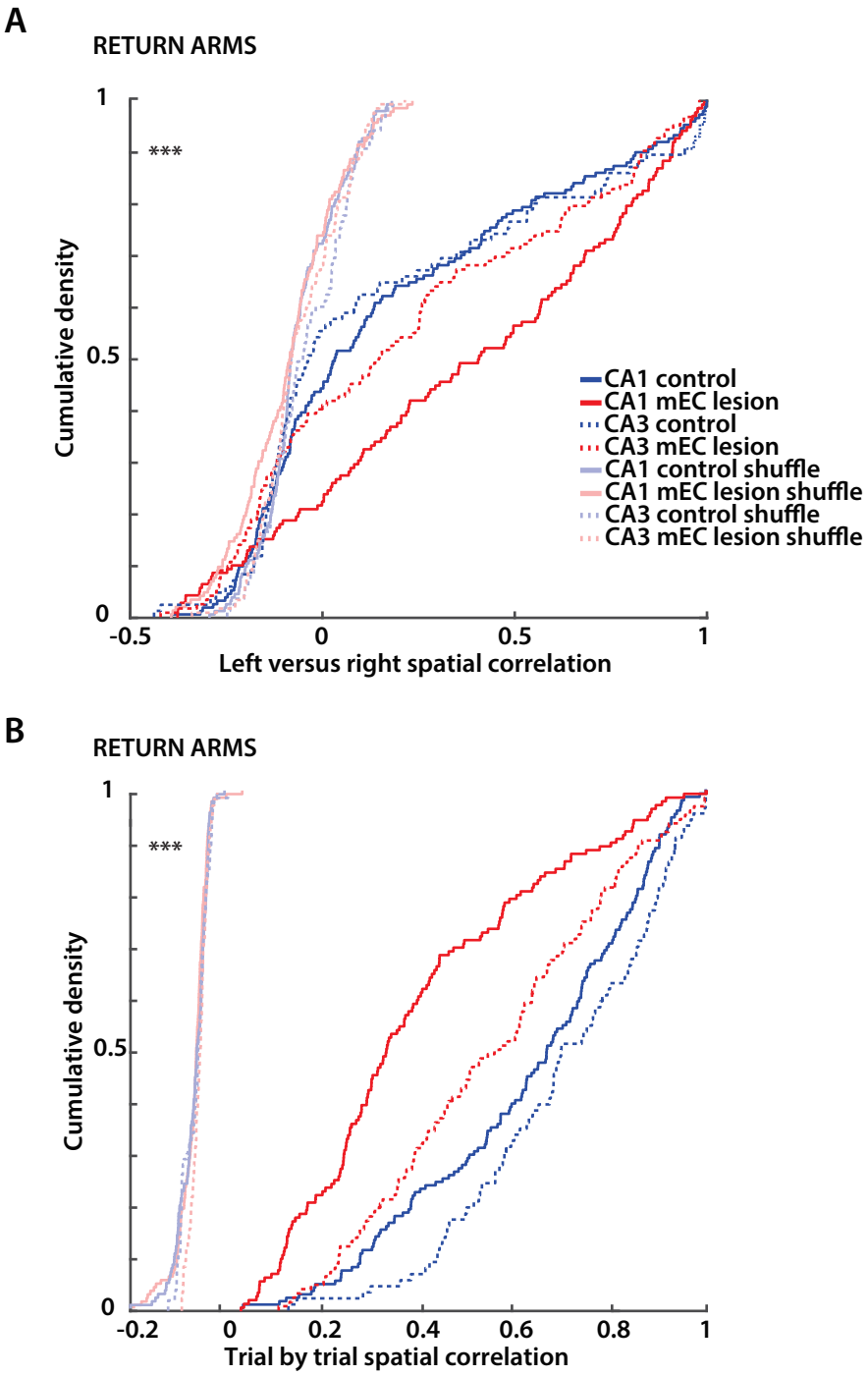

Figure S4. Spatial correlations between left and right maze segments and spatial correlations between trials exceeded shuffled values. Related to Figure 3.

(A) Cumulative density function (CDF) for left versus right spatial correlation. Shuffled values were generated by shifting the spatial firing patterns of the two maze segments with respect to each other. All groups were different than their shuffled distribution (all p values < 0.0001, KS tests). (B) Same as for A, but for the trial-by-trial spatial correlation, which is a measurement for consistency of spatial firing patterns. All groups were different than their shuffled distribution (all p values < 0.0001, KS tests).

FIGURE S5

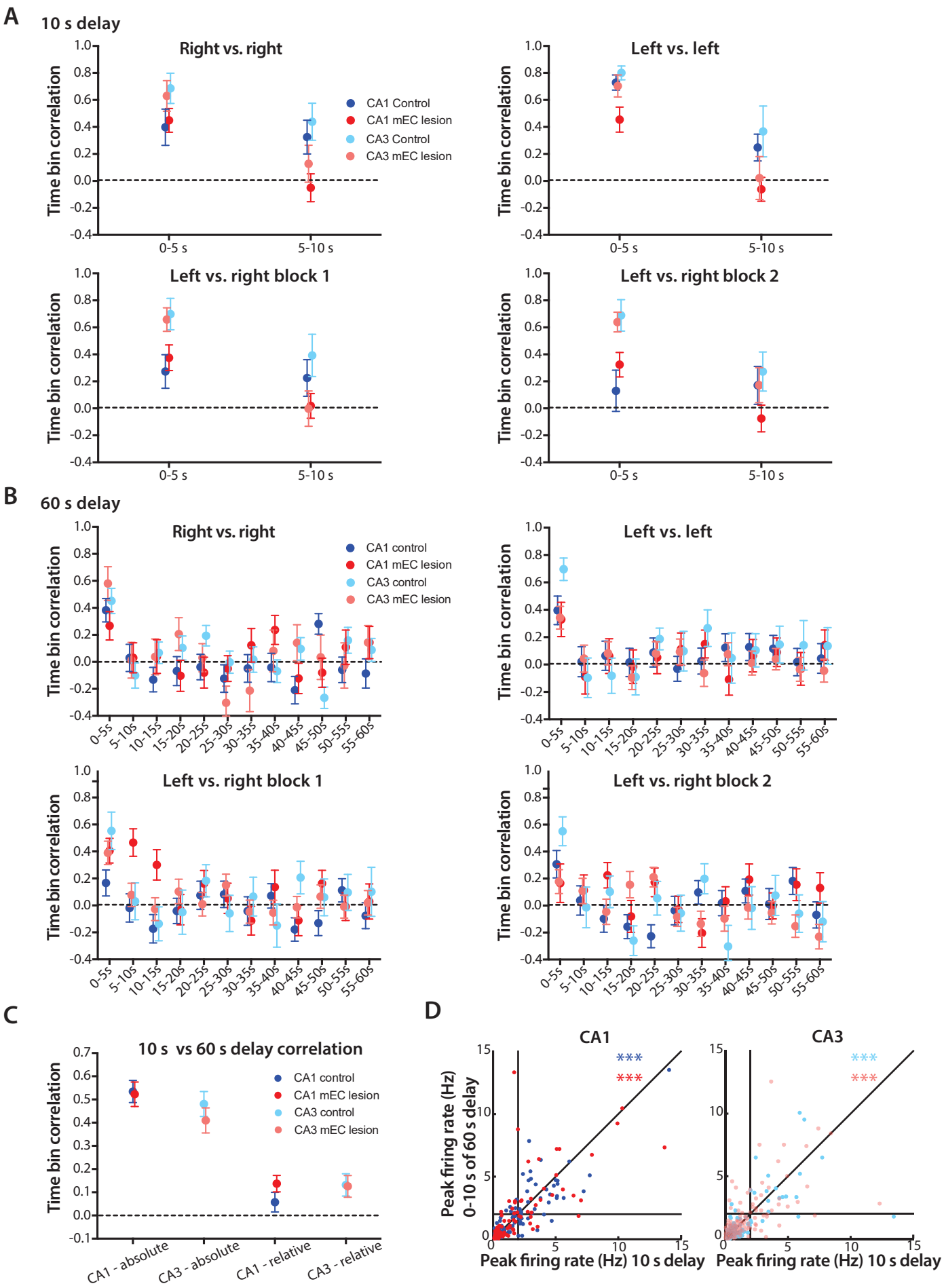
A
10 s delay
Right vs. right
Left vs. left
Left vs. right block 1
Left vs. right block 2
Time bin correlation
CA1 Control
CA1 mEC lesion
CA3 Control
CA3 mEC lesion
0-5 s
5-10 s
B
60 s delay
Right vs. right
Left vs. left
Left vs. right block 1
Left vs. right block 2
CA1 control
CA1 mEC lesion
CA3 control
CA3 mEC lesion
0-5s
5-10s
10-15s
15-20s
20-25s
25-30s
30-35s
35-40s
40-45s
45-50s
50-55s
55-60s
C
10 s vs 60 s delay correlation
CA1 - absolute
CA3 - absolute
CA1 - relative
CA3 - relative
D
CA1
CA3
***
Peak firing rate (Hz) 0-10 s of 60 s delay
Peak firing rate (Hz) 10 s delay

Figure S5. Sequential firing decayed after the first 5 seconds in the delay. Related to Figures 4-6 and Table S4.
(A) For each cell recorded in the 10-s delay condition, correlations between corresponding 0.5 s long time bins were calculated for the first 5 s interval and for the second 5 s interval. The activity during the delay was compared between left-turn and right-turn trials within a block of 10 trials and between blocks of trials of the same type (see Table S4 for statistics). Symbols and error bars are the mean ± SEM. (B) For each cell recorded in the 60-s delay condition, correlations between corresponding 0.5 s long time bins were calculated for each 5 s interval. Blocks and trial-types were compared as in A. (C) Correlations between each time bin in the 10-s delay and the time bins in the first 10 s of the 60-s delay indicate absolute timing (CA1 – absolute and CA3 – absolute). Correlations between each time bin in the 10-s delay and the time bins of the 60-s delay compressed into 10 s indicate relative timing (CA1 – relative and CA3 – relative). While there were no significant differences between groups within a timing condition, all comparisons between absolute and relative timing were significant (all p values < 0.001, Mann-Whitney tests). (D) Peak firing rate of each cell in the 10-s delay compared with the peak firing rate of each cell in the first 10 s of the 60-s delay for CA1 (left) and CA3 (right). Each dot represents a cell, and vertical and horizontal lines correspond to the 2 Hz threshold above which cells were considered to be active. Cells were more likely jointly active in both delay types than by chance (all *** p values < 0.0001, Chi square test).

FIGURE S6

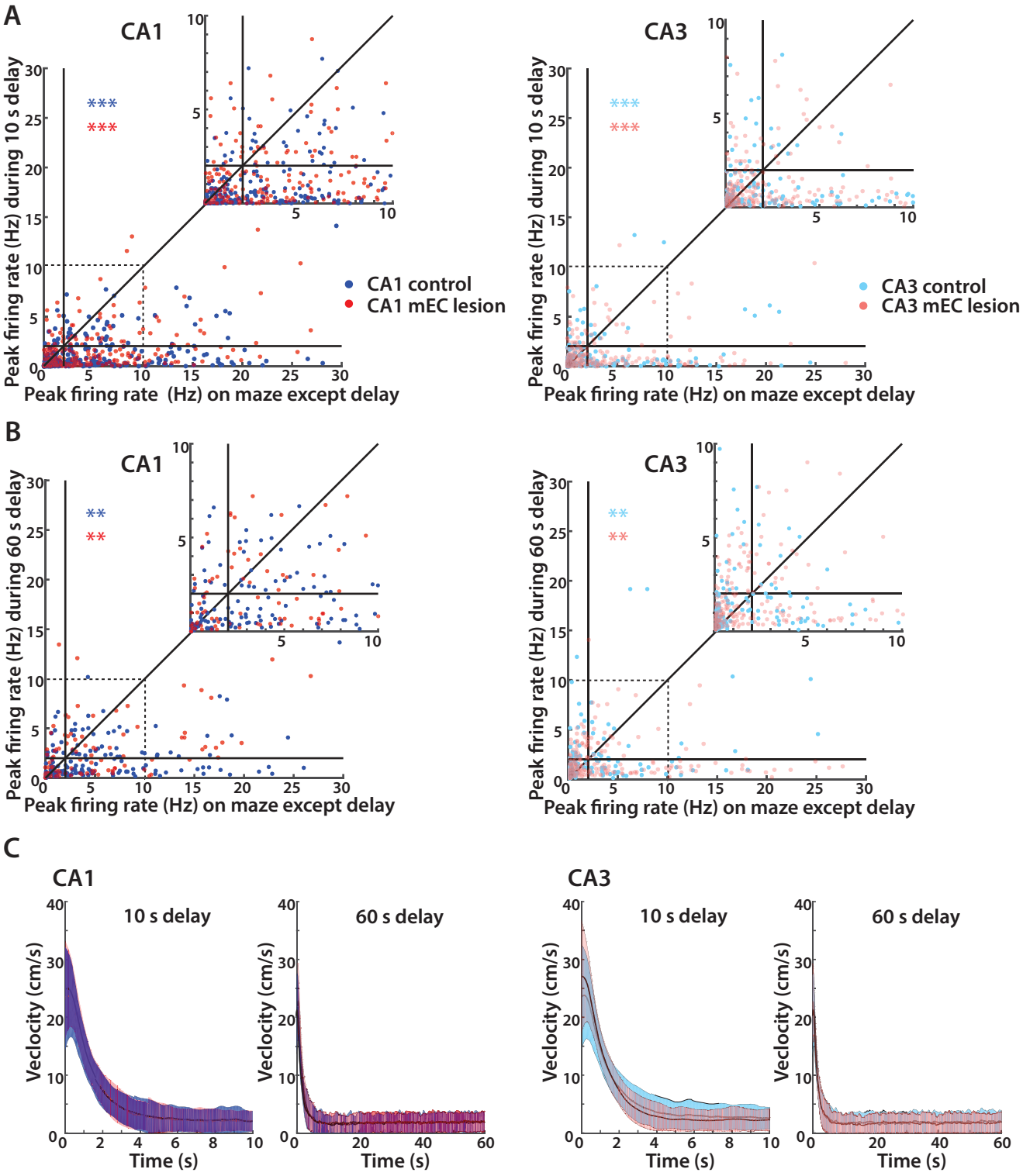

Figure S6. The fraction of cells that were active during the delay and also active on other maze segments was higher than expected by chance. Related to Figures 3-7.

(A) Peak firing rate in the 10-s delay compared to the peak firing rate in the rest of the maze for CA1 (left) and CA3 (right). Each dot represents a cell, and vertical and horizontal lines correspond to the 2 Hz threshold above which cells were considered to be active. Insets show the same data as inside the stippled box (0 Hz to 10 Hz). A higher fraction of cells than expected by chance was active in the delay as well as on other segments on the maze (*** p values < 0.001, Chi square test). (B) Same as A, but for the 60 s delay. Again, a higher fraction of cells than expected was active in both the delay and on other maze segments (** p values < 0.01, Chi square test). (C) Average velocity over time during the delay in CA1 (left) and CA3 (right) recordings. Lines indicate the mean and color shades show ±1 standard deviation. The plots show that rats were immobile after the first 5 seconds in the delay.

FIGURE S7

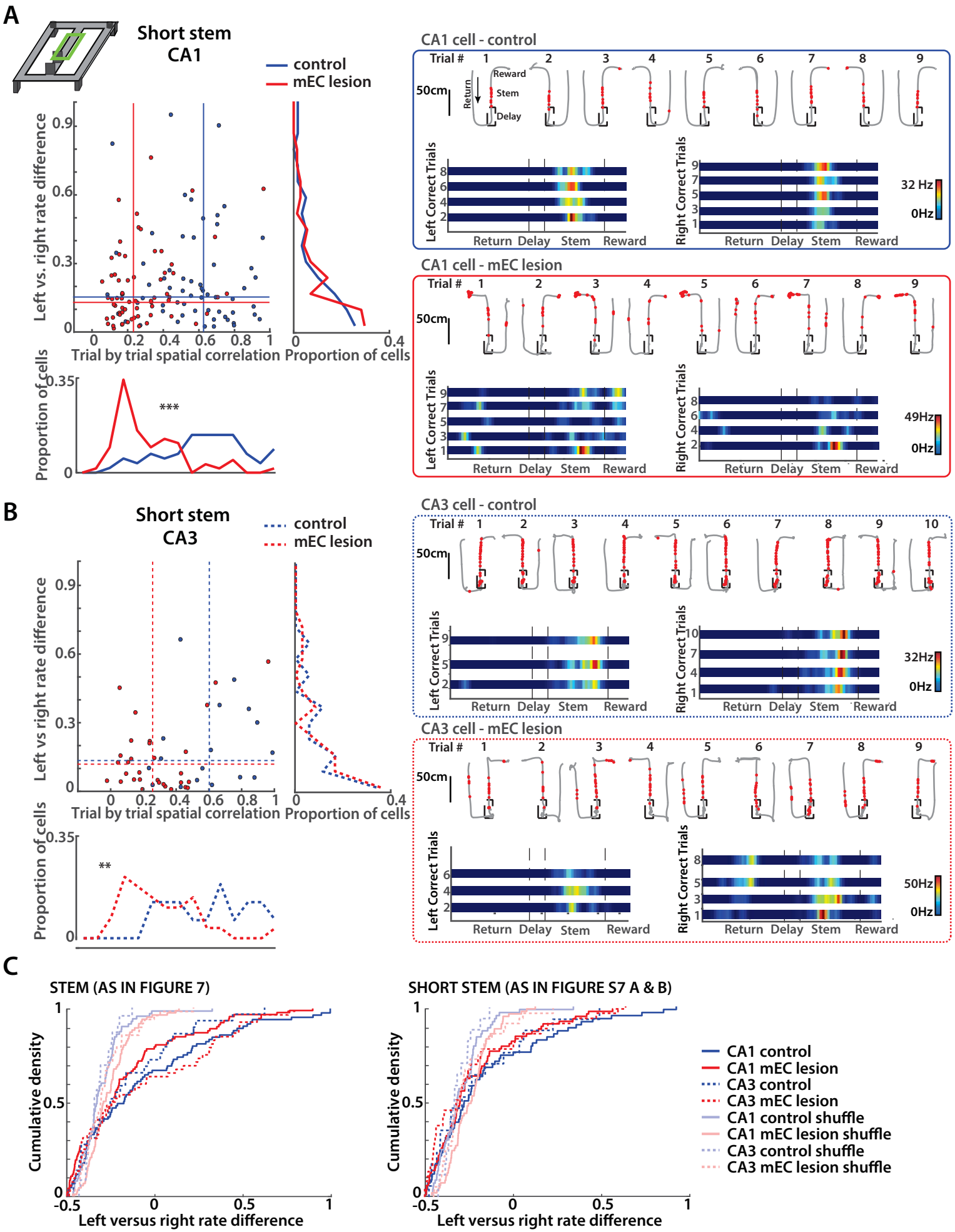
A
Short stem
CA1
control
mEC lesion
Left vs. right rate difference
Trial by trial spatial correlation
Proportion of cells
***
CA1 cell - control
CA1 cell - mEC lesion
Trial #
50cm
Return
Stem
Delay
Reward
Left Correct Trials
Right Correct Trials
32 Hz
0Hz
49Hz
B
Short stem
CA3
CA3 cell - control
CA3 cell - mEC lesion
**
C
STEM (AS IN FIGURE 7)
SHORT STEM (AS IN FIGURE S7 A & B)
Cumulative density
Left versus right rate difference
CA1 control
CA1 mEC lesion
CA3 control
CA3 mEC lesion
CA1 control shuffle
CA1 mEC lesion shuffle
CA3 control shuffle
CA3 mEC lesion shuffle

Figure S7. Fewer cells differentiated between left and right trajectories in the central part of the stem compared to the stem including the segment before the choice point. Related to Figure 7 and Table S2.
(A) (Left) For the center (i.e., short) segment on the stem, CA1 rate difference between correct left and right trials on the stem (left vs. right, vertical axis) and spatial correlation between single trials with the same turn direction (trial-by-trial, horizontal axis). Data for the trial-wise spatial correlations are summarized in the histogram on the bottom (trial-by-trial, *** $p < 0.001$, KS test), and data for the rate differences are summarized to the right (left vs. right rate difference, n.s., KS test). The median values of each group (control and mEC lesion) are shown as horizontal and vertical lines within the scatterplot. (Right) Example CA1 cells from a control and an mEC-lesioned rat. Top row of each example are single correct and incorrect trials (path in grey, spike locations as red dots) and bottom row are linearized rate maps of correct left and correct right trials. (B) Same as A, but for CA3 cells. As for CA1, trial-wise spatial correlations were decreased by the mEC lesion (bottom: ** $p < 0.01$, KS test). However, the proportion of cells that showed differences in firing between left-turn and right-turn trials in the proximal stem segment did not differ between control and mEC-lesioned rats (n.s., KS test), as also observed for the entire stem (see Figure 7). (C) Cumulative density function (CDF) of left versus right rate differences in the extended stem (including the segment before the choice point, as analyzed in Figure 7) and the short stem (as in the remainder of this figure). Shuffles by trial type for each condition are also shown in each plot. In the extended stem, real data were always different from their shuffle (all $p < 0.05$, KS tests). In the short stem, the CA1 rate differences in the mEC lesion group were not different from shuffled data, and CA3 rate differences in the control group were not different from shuffled data (n.s., KS tests; all other conditions: $p < 0.05$, KS tests).

SUPPLEMENTAL TABLES

Table S1. Statistical analysis of spatial alternation behavior in control, mEC lesion and mEC+H lesion groups. Related to Figure 1 and 6.

DAYS 1-7

TWO-WAY ANOVA

Source of variation	F (DFn, DFd)	p value
Interaction	F (4, 51) = 9.45	p < 0.0001
Delay	F (2, 51) = 80.50	p < 0.0001
Group	F (2, 51) = 18.63	p < 0.0001

TUKEY'S TEST

Delays	Comparisons	Mean Diff.	95% CI of diff.	P value summary	Adjusted p Value
no delay	Control vs. mEC lesion	-2.47	-13.21 to 8.26	ns	0.84
	Control vs. mEC+H lesion	-6.11	-17.94 to 5.72	ns	0.43
	mEC lesion vs. mEC+H lesion	-3.63	-15.78 to 8.52	ns	0.75
10 s delay	Control vs. mEC lesion	7.12	-3.62 to 17.86	ns	0.26
	Control vs. mEC+H lesion	25.04	13.21 to 36.86	***	< 0.0001
	mEC lesion vs. mEC+H lesion	17.92	5.77 to 30.07	**	0.0023
60 s delay	Control vs. mEC lesion	19.01	8.27 to 29.74	***	0.0002
	Control vs. mEC+H lesion	32.68	20.85 to 44.51	***	< 0.0001
	mEC lesion vs. mEC+H lesion	13.67	1.52 to 25.82	*	0.024

DAYS 8-14

TWO-WAY ANOVA

Source of variation	F (DFn, DFd)	P value
Interaction	F (4, 51) = 15.67	p < 0.0001
Delay	F (2, 51) = 133.40	p < 0.0001
Group	F (2, 51) = 36.82	p < 0.0001

TUKEY'S TEST

Delays	Comparisons	Mean Diff.	95% CI of diff.	P value summary	Adjusted p Value
no delay	Control vs. mEC lesion	-2.02	-12.85 to 8.81	ns	0.10
	Control vs. mEC+H lesion	-5.32	-17.25 to 6.61	ns	0.87
	mEC lesion vs. mEC+H lesion	-3.31	-15.56 to 8.95	ns	0.99
10 s delay	Control vs. mEC lesion	9.62	-1.21 to 20.45	ns	0.12
	Control vs. mEC+H lesion	28.39	16.47 to 40.32	***	< 0.0001
	mEC lesion vs. mEC+H lesion	18.78	6.52 to 31.03	***	0.0003
60 s delay	Control vs. mEC lesion	14.95	4.12 to 25.78	**	0.0013
	Control vs. mEC+H lesion	31.64	19.71 to 43.57	***	< 0.0001
	mEC lesion vs. mEC+H lesion	16.69	4.44 to 28.95	**	0.0016

DAYS 15-20

TWO-WAY ANOVA

Source of variation	F (DFn, DFd)	p value
Interaction	F (4, 45) = 23.86	p < 0.0001
Delay	F (2, 45) = 162.00	p < 0.0001
Group	F (2, 45) = 61.67	p < 0.0001

TUKEY'S TEST

Delays	Comparisons	Mean Diff.	95% CI of diff.	P value summary	Adjusted p Value
no delay	Control vs. mEC lesion	2.86	-6.04 to 11.76	ns	0.98
	Control vs. mEC+H lesion	-5.56	-17.20 to 6.09	ns	0.82
	mEC lesion vs. mEC+H lesion	-8.41	-20.28 to 3.46	ns	0.36
10 s delay	Control vs. mEC lesion	10.46	1.56 to 19.36	*	0.011
	Control vs. mEC+H lesion	37.60	25.96 to 49.25	***	< 0.0001
	mEC lesion vs. mEC+H lesion	27.14	15.27 to 39.01	***	< 0.0001
60 s delay	Control vs. mEC lesion	11.46	2.56 to 20.36	**	0.0037
	Control vs. mEC+H lesion	36.18	24.54 to 47.83	***	< 0.0001
	mEC lesion vs. mEC+H lesion	24.72	12.85 to 36.59	***	< 0.0001

Table S2. Number of active cells on the stem and number of cells that are differentially active for left versus right turns in CA1 and CA3. Related to Figure 6 and S6.

FIGURE-8 LOCATION	ACTIVITY	GROUP	CA1 CELLS	CA3 CELLS
Entire stem	Active	Control	85	29
		mEC lesion	91	52
	Differentially active	Control	28	8
		mEC lesion	20	15
Proximal stem	Active	Control	62	17
		mEC lesion	76	31
	Differentially active	Control	15	4
		mEC lesion	11	5
Distal stem	Active	Control	23	12
		mEC lesion	15	21
	Differentially active	Control	13	4
		mEC lesion	9	10

Table S3. Linear regression analyses per group and per delay condition. Behavioral performance during the recording phase did not depend on the parasubiculum or mEC lesion volume. Related to Figure 1 and S4.

	Damage	Performance	R square	P value summary	P value
mEC lesion group	% mEC	no delay	0.31	ns	0.10
		10 s delay	0.10	ns	0.33
		60 s delay	0.05	ns	0.63
	% parasubiculum	no delay	0.03	ns	0.65
		10 s delay	0.10	ns	0.36
		60 s delay	0.04	ns	0.67
mEC+H lesion group	% mEC	no delay	0.60	ns	0.13
		10 s delay	0.95	**	0.010
		60 s delay	0.31	ns	0.33
	% parasubiculum	no delay	0.12	ns	0.57
		10 s delay	0.55	ns	0.15
		60 s delay	0.76	ns	0.060

Table S4. Statistical analysis of time bin correlations during the 10 and 60 s delays using 5 s intervals (only significant comparisons are shown). Related to Figure 4, 5 and S5.

CA1 - 10 s Delay

TWO-WAY ANOVA: R-R Trials

Source of Variation	% of total variation	P value	P value summary
Interaction	3.05	0.06	ns
Elapsed time	5.52	0.01	*
Group	1.77	0.15	ns

TWO-WAY ANOVA: L-L Trials

Source of Variation	% of total variation	P value	P value summary
Interaction	0.02	0.86	ns
Elapsed time	20.29	< 0.0001	***
Group	6.95	0.0026	**

TWO-WAY ANOVA: L1-R1 Trials

Source of Variation	% of total variation	P value	P value summary
Interaction	1.84	0.17	ns
Elapsed time	3.15	0.07	ns
Group	0.21	0.64	ns

TWO-WAY ANOVA: L2-R2 Trials

Source of Variation	% of total variation	P value	P value summary
Interaction	3.20	0.07	ns
Elapsed time	2.13	0.13	ns
Group	0.04	0.83	ns

CA3 - 10 s Delay

TWO-WAY ANOVA: R-R Trials

Source of Variation	% of total variation	P value	P value summary
Interaction	1.50	0.32	ns
Elapsed time	12.95	0.0043	**
Group	3.10	0.15	ns

TWO-WAY ANOVA: L-L Trials

Source of Variation	% of total variation	P value	P value summary
Interaction	1.16	0.35	ns
Elapsed time	23.24	< 0.0001	***
Group	3.65	0.10	ns

CA1 - 60 s delay

TWO-WAY ANOVA: R-R Trials

Source of Variation	% of total variation	P value	P value summary
Interaction	3.20	0.07	ns
Elapsed time	2.13	0.13	ns
Group	0.04	0.83	ns

TWO-WAY ANOVA: L-L Trials

Source of Variation	% of total variation	P value	P value summary
Interaction	0.75	0.93	ns
Elapsed time	2.66	0.09	ns
Group	0.03	0.64	ns

TWO-WAY ANOVA: L1-R1 Trials

Source of Variation	% of total variation	P value	P value summary
Interaction	2.86	0.040	*
Elapsed time	4.28	0.0018	**
Group	1.41	0.0017	**

SIDAK'S TEST

Between Group Comparison	Time Bin	Mean Diff.	95% CI of diff.	P value summary	Adjusted P Value
CA1 mEC and CA1 Control	5-10s	0.48	0.070 to 0.90	*	0.010
	10-15s	0.47	0.037 to 0.91	*	0.023

Within Group Comparison	Group	Mean Diff.	95% CI of diff.	P value summary	Adjusted P Value
5-10s vs. 30-35s	CA1 mEC Lesion	0.58	0.056 to 1.10	*	0.013
5-10s vs. 40-45s		0.58	0.06 to 1.10	*	0.012

TWO-WAY ANOVA: L2-R2 Trials

Source of Variation	% of total variation	P value	P value summary
Interaction	2.69	0.08	ns
Elapsed time	2.98	0.04	*
Group	0.27	0.17	ns

CA3 - 60 s delay

TWO-WAY ANOVA: R-R Trials

Source of Variation	% of total variation	P value	P value summary
Interaction	2.08	0.22	ns
Elapsed time	7.58	< 0.0001	***
Group	0.00009	0.98	ns

TWO-WAY ANOVA: L-L Trials

Source of Variation	% of total variation	P value	P value summary
Interaction	1.66	0.43	ns
Elapsed time	5.88	< 0.0001	***
Group	0.49	0.07	ns

TWO-WAY ANOVA: L1-R1 Trials

Source of Variation	% of total variation	P value	P value summary
Interaction	1.28	0.67	ns
Elapsed time	4.99	0.0006	***
Group	0.027	0.67	ns

TWO-WAY ANOVA: L2-R2 Trials

Source of Variation	% of total variation	P value	P value summary
Interaction	3.04	0.036	*
Elapsed time	5.33	0.0002	***
Group	0.045	0.58	ns

SIDAK'S TEST

Within Group Comparison	Group	Mean Diff.	95% CI of diff.	Summary	Adjusted P Value
20-25s vs. 55-60s	CA3 mEC Lesion	0.44	0.023 to 0.86	*	0.026
0-5s vs. 15-20s		0.81	0.15 to 1.47	**	0.0025
0-5s vs. 35-40s	CA3 Control	0.85	0.19 to 1.51	***	0.001
0-5s vs. 55-60s		0.67	0.011 to 1.33	*	0.041